doi: 10.2166/9781789061932_0001

Chapter 1

An introduction to photocatalysis

Mohammad Reza Boskabadi[1], Vincent Rogé[2], Alireza Bazargan[3], Hamed Sargazi[3] and Emanuele Barborini[2]*

[1]School of Chemical Engineering, College of Engineering, University of Tehran, Tehran, Iran
[2]The Nanomaterial and Nanotechnologies Unit, Materials Research and Technology Department, Luxembourg Institute of Science and Technology, Luxembourg
[3]School of Environment, College of Engineering, University of Tehran, Tehran, Iran
**Corresponding author: emanuele.barborini@list.lu*

ABSTRACT

In this chapter the principles behind photocatalytic water and wastewater treatment as well as water splitting for energy production (producing oxygen and hydrogen gas) are discussed. The mechanisms involved in the generation of charge carriers in semiconductors and their behavior towards pollutant degradation or water splitting are also outlined. As conferred, a variety of organic molecules have been degraded by photocatalysis, including dyes, phenols, nitrogen-containing molecules, pesticides, and pharmaceuticals. Characterization techniques with which lifetimes and spatial distributions of charge carriers are displayed in photocatalytic materials are touched upon. Additionally, various strategies for improving the photocatalytic activity are discussed as well as the reasons behind the development of such strategies. This includes describing the formation of heterostructures formed between semiconductors as well as the experimental parameters that affect the kinetics of such reactions. A quick summary of the operational parameters that affect the photocatalytic process reviews the effects of pH, temperature, presence of oxidants, concentration of the target pollutant, catalyst loading, and light intensity and wavelength.

1.1 PRINCIPLES OF PHOTOCATALYSIS

With increasing worldwide interest in environmental issues such as global warming, water/air pollution and waste management, many efforts are being made to find cost effective and sustainable processes for energy production, pollution elimination or recycling. The most abundant energy source available on earth is sunlight. Consequently, engineering efficient solar technologies is

a critical step towards carbon-free energy production. In principle, the solar energy received on earth every day should be enough to meet all of mankind's energy needs. However, solar systems are not yet efficient enough to convert and store the required energy. For this reason, solar energy is an exciting and rapidly growing research topic attracting scientists' interest in different fields, including electricity production with photovoltaic or photothermal solar panels, hydrogen production with photocatalytic/photo-electrocatalytic water splitting, and solar photocatalytic water treatment.

Photocatalytic materials are materials that are able to convert an incident photon into a consumable or storable energy source, through the creation of an electron/hole pair at the photocatalyst level. From a general point of view, a photocatalyst is a catalyst that exhibits its catalytic properties under light irradiation, via absorption of photons. Such photocatalytic systems exist in nature, like in the photosynthesis process occurring in green leaves, where chlorophyll acts as a photocatalyst allowing the conversion of water and CO_2 into O_2 and sugars. Engineered photocatalysts tend to mimic this natural process by employing photogenerated electron/holes to create energetic radicals, which can be used for various applications such as water treatment or splitting water into O_2 and H_2.

The photocatalytic water treatment process is part of a broader family called advanced oxidation processes (AOPs). They all involve the production and utilization of highly oxidative OH· radicals to fragment and decompose organic molecules. Targeted molecules could be residual xenobiotics, dyes, pesticides or herbicides present in the wastewater due to human consumption or industrial activity [1]. AOPs are currently applied in many wastewater treatment plants, particularly photolytic and photo-Fenton processes. In photolytic processes, sacrificial molecules such as hydrogen peroxide, H_2O_2, or ozone, O_3, are irradiated under powerful germicidal ultraviolet (UV) light (254 nm) in order to produce oxidative radicals. In the photo-Fenton process, catalytic ferrous ions (Fe^{2+} or Fe^{3+}) are added with H_2O_2 under UV light, in order to generate OH· radicals more efficiently [2]. The drawback of these processes is that they use expensive and energy-consuming UV lights, and catalysts like ferrous ions operate suitably in a narrow acidic pH range (2.8–3.5) in order to avoid the precipitation of inactive iron oxyhydroxide species [3]. Thus, a pH neutralization of the treated water with alkaline chemicals is necessary.

To overcome those limitations, heterogeneous photocatalysis appears as a promising alternative. In this process, photocatalysts are solid materials like particles/nanoparticles suspended in water or supported on a substrate like a membrane. No sacrificial or additional chemicals are needed. The advantage of supported photocatalysts over the suspended ones is that no filtration process is needed afterwards. Nevertheless, the specific surface area of suspended photocatalysts is generally higher than that of supported ones, leading to improved degradation properties. Currently, the most effective photocatalysts operate in the UV range of the light spectrum. Thus, they suffer the same limitations as the photolytic or photo-Fenton processes cited above, that is the need for energy-consuming UV lights. UV light represents only a small percentage (5%) of the solar light passing through the atmosphere. Most of the

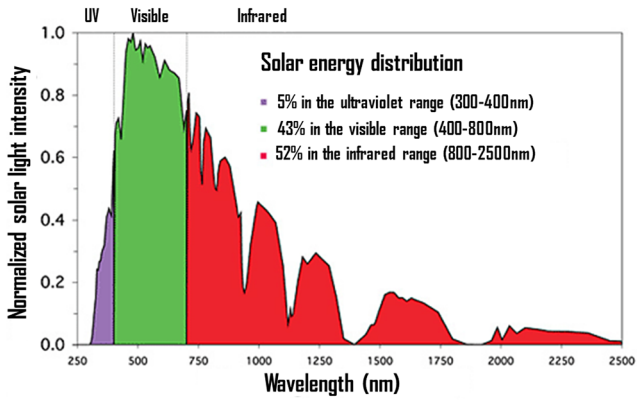

Figure 1.1 Spectrum representing the solar light received at the surface of the earth. Reprinted from [4].

solar light received at the surface of earth is in the visible (43%) and infrared region (52%) (Figure 1.1). Considering this, one can easily understand the crucial need for investing in research for the fabrication of visible-light active materials.

In addition to the ability to operate in the visible range, other parameters are being studied to enhance the performance of photocatalysts, like improving the lifetime of charge carriers and their mobility/availability at the surface.

1.2 MECHANISM AND CHARACTERIZATION OF THE PHOTOCATALYTIC PROCESS

1.2.1 Photocatalytic mechanism

The photocatalytic degradation process is schematically shown in Figure 1.2 [5]. Photons having energy larger than the photocatalyst's band gap are absorbed by the photocatalyst: an electron from its valence band is ejected into its conduction band, thus an electron/hole (e^-/h^+) pair is created. If the positive charge carrier

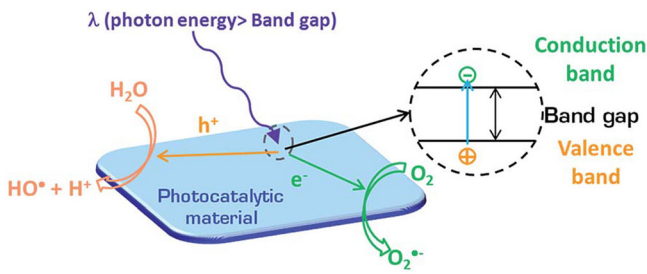

Figure 1.2 Schematic representation of a photocatalytic initiation process. Reprinted with permission from [5].

h^+ remaining in the valence band of the photocatalyst has an oxidation potential above 2.31 V/NHE (normal hydrogen electrode), (potential of the couple OH·/H^+, H_2O) at pH = 0, it can oxidize water into H^+ and OH·. If the negative charge carrier e^- remaining in the conduction band of the photocatalyst has a potential below 0.92 V/ENH (potential of the oxygen reduction in $O_2^{\cdot-}$) at pH = 0 [6], it can reduce O_2 into $O_2^{\cdot-}$. With an oxidation potential of 2.31 V/ENH at pH = 0, OH· radicals are energetic enough to break covalent C–C bonds in organic molecules, while $O_2^{\cdot-}$ radicals have a reductive potential sufficient to reduce water into hydrogen peroxide (H_2O_2). Hydrogen peroxide decomposes under UV light into 2 OH·. The photo-generation of OH· is direct during the water oxidation with h^+, while it is a two-step process during the water reduction with e^-. Consequently, photocatalytic degradations of organic compounds are more efficiently driven by the oxidative OH· generation with h^+.

The overall mechanism for the photocatalytic degradation of organic compounds can be written as follows:

$$\text{Photocatalyst} + h\nu = \text{Photocatalyst}\ (h_{(vb)}^{+} + e_{(cb)}^{-})$$

$$H_2O + h_{(vb)}^{+} \rightarrow H^+ + OH\cdot \tag{1.1}$$

$$e_{(cb)}^{-} + O_2 \rightarrow O_2^{\cdot-} \tag{1.2}$$

$$O_2^{\cdot-} + H^+ \rightarrow HO_2\cdot \tag{1.3}$$

$$O_2^{\cdot-} + HO_2^{\cdot} + H^+ \rightarrow H_2O_2 + O_2 \tag{1.4}$$

$$H_2O_2 + h\nu \rightarrow 2\,OH\cdot \tag{1.5}$$

$$OH\cdot + \text{organic compounds} \rightarrow CO_2 + H_2O + \cdots \tag{1.6}$$

The photocatalytic water splitting follows the same mechanism. In this case, photocatalysts must generate negative charge carriers e^- with oxidation potentials more reductive than 0 V/NHE at pH = 0 (the oxidation potential of the couple H^+/H_2); and positive charge carriers h^+ with oxidation potentials more oxidative than 1.23 V/NHE at pH = 0 (the oxidation potential of the couple O_2/H_2O). The overall water splitting can be described as follows [7]:

$$2H_2O \rightarrow 2H_2 + O_2 (\Delta G^\circ = 238\,\text{kJ.mol}^{-1}) \tag{1.7}$$

With half-reactions:

$$2H^+ + 2e_{(cb)}^{-} \rightarrow H_2 \tag{1.8}$$

$$2H_2O + 4h_{(vb)}^{+} \rightarrow O_2 + 4H^+ \tag{1.9}$$

With a large positive change in the Gibbs free energy (238 kJ.mol^{-1}), water splitting is an uphill reaction that needs to be activated with catalysts (or photocatalysts). Since the energy needed to split the water molecule is 1.23 eV (1.23 V/NHE at pH = 0), the water splitting process can theoretically be performed with photocatalysts absorbing photons in the infrared range

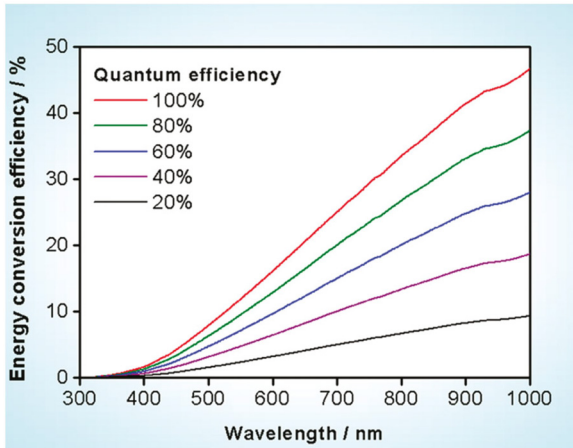

Figure 1.3 Calculated energy conversion efficiency versus wavelength for different quantum efficiencies. Reprinted from [8].

(indeed photon energies higher than 1.23 eV correspond to wavelengths smaller than 1010 nm). Based on calculations using fixed quantum efficiencies of photocatalysts, K. Maeda [8] showed that the solar energy conversion effectiveness increases with the increasing wavelength of photons, from the UV to the infrared part of the light spectrum (Figure 1.3). This is explained by the highest number of photons available when the wavelength increases (Figure 1.1). Results presented in Figure 1.3 endorse the necessity of developing visible light active photocatalysts.

1.2.2 Lifetime and mobility characterization of photo-excited charge carriers

As the photocatalytic process requires the photo-production of e^-/h^+ pairs and their interaction with the target molecules, the understanding of pair recombination times and mobilities is of paramount importance in order to rationally design efficient photocatalysts. The global timescale of a photocatalytic process extends over hundreds of milliseconds to a few seconds, as presented in Figure 1.4 [9]. Typically, photon absorption and the formation/diffusion of charge carriers e^-/h^+ are very quick steps performed within a few picoseconds (ps). Then, the charge carriers diffuse within nanoseconds (ns) to microseconds (μs). In several materials, the nanosecond to microsecond range is also the timescale range for recombination of charge carriers [10, 11]. The oxidation/reduction process, following the transport of charge carriers at the surface of the photocatalyst and involving the mass transfer of the water/pollutants at the interface, is the last process occurring in a few hundreds of milliseconds (ms) to seconds (s).

In the photocatalytic process mechanism, lifetimes and mobilities of carriers depend on multiple factors like the chemical environment, the driving force of transport energetic charge to absorbed reactant molecules, and the

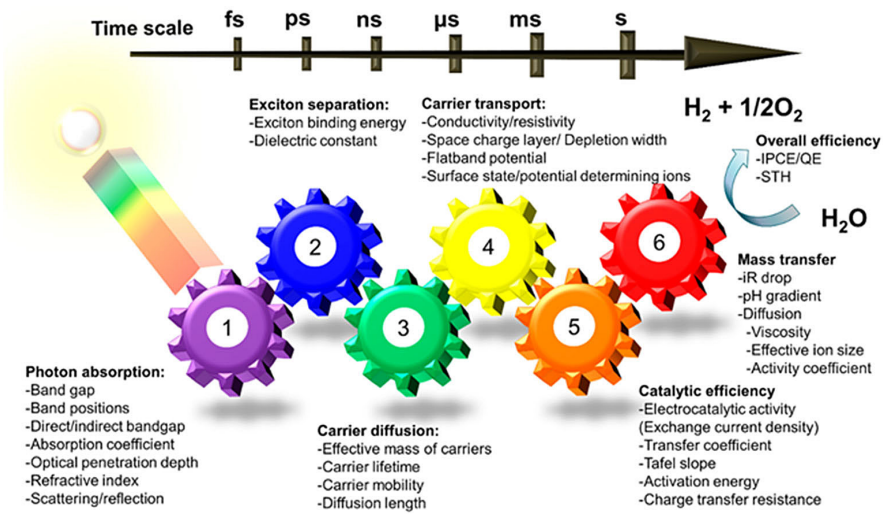

Figure 1.4 Timescale for photocatalytic water splitting. IPCE: incident photon to current efficiency, QE: quantum efficiency; STH: solar-to-hydrogen. Reprinted from [9].

lifetime of highly reactive intermediates [11]. Experimental techniques able to precisely characterize excitation/recombination kinetics (ps-µs), charge separation and transfer (ps-ns), surface reactions (µs-ms) or diffusion mean free path have emerged in recent years. Among them, one can distinguish optical spectroscopies and electron or scanning probe microscopies, like time resolved photoluminescence/fluorescence (tr-PL), transient absorption spectroscopy (TAS), time resolved microwave conductivity (TRMC), ultra-fast electron microscopy, kelvin probe force microscopy (KPFM) or conductive atomic force microscopy (C-AFM).

Optical processes rely on the principle of time resolved spectroscopy, like pump-probe transient absorption spectroscopy, time resolved microwave conductivity or time resolved photoluminescence. In the transient absorption spectroscopy process, an incident energy source (usually a laser pulse in the visible or infrared range) acts as a pump that excites atoms or electrons and generates a non-equilibrium state. A second light source, weaker than the first one and delayed in time, probes the induced changes in optical constants. It allows the determination of the relaxation time of generated species, with a time resolution directly linked to the pump source used [12]. Thanks to the latest laser technologies, able to deliver laser pulses below 10 fs, the time resolution offered by ultra-fast transient absorption spectroscopy allows the characterization of the early stages of the photocatalytic processes (fs to ns).

Time resolved microwave conductivity is a variant of transient absorption techniques (involving visible or infrared light sources). In this case, microwave or terahertz electromagnetic waves are used as pump sources. The major difference

compared to visible/infrared excitation is that the absorption is directly related to the conductivity of charge carriers created in the material [13], and not to optical transitions from the ground state to non-equilibrium ones. This allows the qualitative and quantitative measurement of changes in microwave absorption resulting from light induced production and decay of charged and dipolar molecular entities [14]. The microwave absorption intensity is a function of the product of the number of mobile charges and their mobilities. This characterization technique unveils evidence on recombination of charge carriers and dynamics, effective mobility, and lifetime and trapping of formed carriers [15], within the femtosecond to nanosecond scale (depending on the probe laser).

Time resolved photoluminescence is a technique close and often complementary to transient absorption spectroscopy. It measures the emitted fluorescence or photoluminescence signal instead of changes in absorption properties (for TAS). Just like transient absorption, the excitation source is a short laser pulse creating non-equilibrium states in the materials [11]. The radiative decay of charge carriers, due to recombination or trapping, is detected with a time resolution from a few picoseconds to microseconds [16, 17]. The complexity of the full photocatalytic process, due to the large timescale involved between the light absorption and the modification of the target molecules (e.g. water splitting or degradation of organic compounds), makes its complete characterization a difficult task. As an example, Dillon *et al.* revealed that four different samples of TiO_2@Au core/shell structures, which were showing different efficiencies toward water splitting, had similar TAS kinetic curves with a longer time delay of around 1.5 ns [18]. This result can be explained by the fact that, at the timescale studied (the nanosecond scale), all four samples had the same properties, but most likely photo-excited charge carriers with longer lifetimes were responsible for the water splitting. Consequently, the study of transient absorption at the nanosecond timescale alone can account for only a part of the photocatalytic process. In order to understand the photocatalytic properties of carbon nitride, R. Godin *et al.* [19] investigated charge trapping and recombination with tr-PL and TAS techniques, over 10 orders of time magnitude. This allowed them to elucidate fundamental excited state processes that dictate the global photocatalytic activity.

In addition to characterization of the carriers' lifetimes and mobilities, the investigation of their spatial distribution and transfer is key to precisely determine active sites on photocatalysts. To this end, AFM-based techniques, such as KPFM or C-AFM, have been shown to be powerful tools. KPFM measures electrostatic forces between the sample and a cantilever, leading to the description of the electric potential distribution of sample surface with nanometric lateral resolution. It is usually adopted in materials science for work function mapping [20] or dopant profile determination within semiconductors [21]. In addition, it can also unveil surface photovoltage under illumination (difference in contact potential under illumination and in the dark) and, consequently, achieve spatially resolved surface photovoltage spectroscopy (SR-SPS) [22]. Using KPFM coupled with standard AFM, A. Jian *et al.* studied the electron transfer in an Au/TiO_2 nanoparticles/thin film system under light irradiation [23]. As depicted in Figure

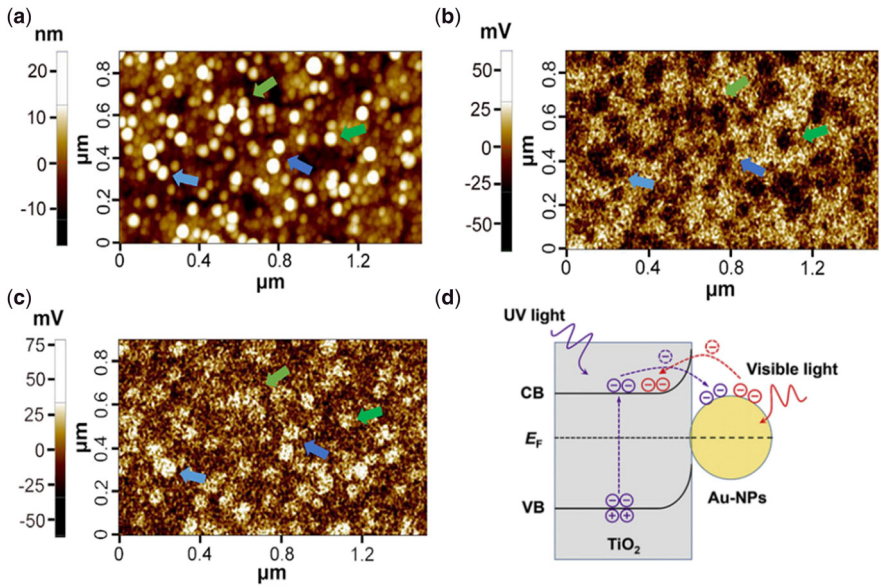

Figure 1.5 (a) AFM topography image, (b) surface potential images of Au/TiO_2 under UV light, (c) surface potential images of Au/TiO_2 under visible light. Arrows with same color identify the same particles in these three images, (d) scheme of the electron migration mechanism under UV or visible light. Figure reproduced from [23].

1.5, the surface charge of gold particles under visible or UV light is determined in situ by KPFM. This technique revealed that under UV light, surfaces of gold nanoparticles were charged negatively (Figure 1.5b), whereas under visible light they were charged positively (Figure 1.5c). Consequently, KPFM measurements help to determine the electron migration mechanism in the Au/TiO_2 system (Figure 1.5d). Under UV light, electrons/holes are photogenerated in the TiO_2 film, and electrons in the conduction band migrate at the gold nanoparticle's surface. When the material is irradiated by visible light, the incident energy is too low to produce electron/hole pairs in the TiO_2, but a localized surface plasmons resonance (LSPR) phenomenon appears at the surface of the gold nanoparticles. Excited electrons from the LSPR migrate from the gold nanoparticle to the TiO_2 film, leading to a positive net charge on the gold surface.

C-AFM measures the local direct current (DC) between the sample and the cantilever. When operated in tapping mode (cantilever resonance oscillation), it offers the possibility of measuring the current–voltage behavior of the sample with nanometric lateral resolution [24], leading to large multidimensional datasets. C-AFM allows correlation between the morphology and the (photo) current response of the photocatalyst [25]. In particular, C-AFM enables the mapping of surface conductivities and charge transfer characteristics at grain boundaries, facet planes or at the interface between two different materials (e.g. heterojunction, co-catalyst). Recently, Eichhorn *et al.* [26] showed that C-AFM

measurements, using back side illumination, allowed for the determination of optoelectronic heterogeneities in $BiVO_4$ photoanodes.

1.2.3 Photocatalysis characterization by organic dye degradation

When one thinks about photocatalytic water treatment, organic dyes, pesticides, herbicides and xenobiotics appear among the most important molecules to eliminate. If the spatiotemporal characterization of charge carriers at the nanometric-microscopic level provide useful pieces of information on photocatalyst properties, macroscopic processes are necessary in order to precisely determine their actual photocatalytic performances. Organic dyes are among the most studied molecules for the determination of photocatalyst degradation performances. Textile and manufacturing industries are responsible for water pollution with many different types of colored dyes, and their elimination is a serious problem to tackle. Dyes can be classified based on their chromophoric group, including azo dyes, acridine dyes, nitro dyes, phenothyazine dyes, xanthene dyes or quinine-amine dyes [27]. Thanks to their chromophoric groups, the photocatalytic degradation of organic dyes can easily be tracked with visible light absorption measurements. The degradation of dyes on photocatalysts usually follows a pseudo-first order reaction kinetic: the Langmuir-Hinshelwood model [28]. This model can be expressed as follows:

$$r = \frac{dC}{dt} = k_r q_x = \frac{k_r KC}{1 + KC} \tag{1.10}$$

in which r denotes the photodegradation rate. The surface on the photocatalyst covered by the target molecules is shown with q_x. The parameters k_r and C are the reaction constant and concentration at time t. K is the adsorption constant which depends on the surface of the catalyst as well as the molecule. If the equation is rearranged it will look as follows:

$$dt = \frac{1 + KC}{k_r KC} dC \tag{1.11}$$

Or,

$$t = \frac{1}{k_r K} \ln \frac{C_0}{C} + \frac{1}{k_r}(C_0 - C) \tag{1.12}$$

Under conditions where the initial concentration of C_0 is negligibly low, Equation (1.12) can be simplified to the following form:

$$\ln \frac{C_0}{C} = k_r Kt = k't \tag{1.13}$$

where k' corresponds to the pseudo-first order constant reaction. In order to simplify the reaction kinetics to the first order, most of the photocatalytic degradation processes of dyes involve low initial concentration and thus the photocatalytic degradation constant is determined based on Equation (1.13).

Rhodamine B (xhantene) [29, 30], methylene blue (phenothiazine) [5, 31] and methyl orange (azo dye) [32] are common dyes used to probe photocatalytic reactions. Their total mineralization (full degradation of the molecule to H_2O and CO_2) can be obtained via the photocatalytic degradation process on photocatalysts [33, 34]. However, not all dyes can be easily mineralized. As an example, dyes containing the triazine group tend to form highly stable cyanuric acid [35]. During the photocatalytic degradation process with colored dyes, the disappearance of the color is usually attributed to the degradation of the molecule. This consideration is often erroneous, as the decoloration is just the consequence of the degradation of the chromophoric group, and not of the full molecule. In azo dyes, the decoloration appears after the attack of the azo bond (C−N=N−) [36]. This is followed by aromatic rings opening, then formation of carboxylic acids which ultimately decarboxylate by the 'photo-Kolbe' reaction to release CO_2 [37]. Consequently, the decoloration of dyes can provide indications of photocatalyst performances, but does not signify the complete mineralization of the molecule. In order to improve the process characterization, total organic carbon (TOC) analysis, which quantitatively determines the amount of carbon in organic molecules present in the water, is often used [38, 39].

1.3 HOMOGENEOUS AND HETEROGENEOUS PHOTOCATALYTIC PROCESSES

Generally, homogeneous systems are those in which the catalyst is in the same phase (gas or liquid) as the reactants. Conversely, in heterogeneous systems, the catalyst is not in the same phase as the reactants, such as the use of solid and/or powdered catalysts in a liquid reaction mixture. For example, the heterogeneous reaction employing TiO_2/UV and the homogeneous reaction using Fe^{2+}/H_2O_2 have attracted a lot of interest [40].

1.3.1 Homogeneous example: photo-Fenton reaction

Fenton's reaction is named after Henry Fenton, who observed the activation of H_2O_2 in the presence of iron for the oxidation of tartaric acid [41]. The classical mechanism of the photo-Fenton process is a simple redox reaction in which Fe^{2+} is converted to Fe^{3+} and H_2O_2 to a hydroxyl ion (OH^-) and hydroxyl radical ($OH\cdot$) with a strong oxidation potential ($E_0 = 2.73$ V vs. NHE) [42]. Following this reaction (Equation (1.14)), the generated ferric ion can be converted back to ferrous ions by H_2O_2 (Equation (1.15)). The reduction of Fe^{3+} as per Equation (1.15) with a reaction constant of 0.02 $M^{-1}s^{-1}$ is much slower than the oxidation of Fe^{2+} as per Equation (1.14) with a reaction constant of 40–80 $M^{-1}s^{-1}$. Thus, the rate limiting step is identified, and large amounts of initial Fe^{2+} ions are required to mineralize organic pollutants [43].

$$Fe^{2+} + H_2O_2 \rightarrow Fe^{3+} + OH^- + OH\cdot \quad (1.14)$$

$$Fe^{3+} + H_2O_2 + H_2O \rightarrow Fe^{2+} + H_3O^+ + HO_2^{\cdot -} \quad (1.15)$$

$$OH\cdot + H_2O_2 \rightarrow HO_2^{\cdot -} + H_2O \quad (1.16)$$

$$OH\cdot + Fe^{2+} \rightarrow Fe^{3+} + OH^- \quad (1.17)$$

Many studies have focused on the photo-Fenton treatment of water and wastewater. For example, Ahile *et al.* (2021) sought to answer the question 'Is iron-chelating in a homogeneous photo-Fenton process at neutral pH suitable for purifying the output current from the biological secondary purification system?'. In the study, oxalic acid (OA), nitrileutria acetic acid (NTA), ethylenediamine acid (EDDS), citric acid (CA), and ethylenediaminetetraacetic acid (EDTA) were used as chelating agents at pH = 7 while a homogeneous photo-Fenton process took place. The results were reported based on disinfection and bacterial regrowth leading to the preferential order of EDTA > OA > NTA > CA > EDDS. It was also observed that all iron chelates caused an increase in chemical oxygen demand (COD) in the effluent, for which the effect of EDDS was higher than other compounds [44].

1.3.2 Heterogeneous photocatalytic reaction examples

With the discovery of the photocatalytic properties of TiO_2, research regarding heterogeneous photocatalysis has become commonplace. The heterogeneous photocatalytic mechanism begins primarily with the ability of semiconductors to produce charge carriers. This is followed by the production of hydroxyl free radicals, which eventually leads to the breakdown of organic compounds to H_2O and CO_2 [45]. The most attractive features of this process are [46]:

- Pollutants can be completely degraded to CO_2 and other minerals
- The process usually takes place at ambient conditions
- The only requirement for the reaction to start is the presence of oxygen and energy received above the band gap energy, both of which are abundantly available
- Various types of inert matrices, including glass, polymers, carbon nanotubes, and graphene oxides, can be used as catalyst supports
- The catalyst is inexpensive, non-toxic, and reusable

The heterogeneous photocatalytic mechanism involves a chain of oxidation and reduction reactions at the photocatalyst level. In a semiconductor, the distance between the last electron-occupied band (capacitance band) and the first empty electron band (conduction band) is called the band gap. When the energy of the photons colliding with the semiconductor is greater than or equal to the energy of the gap band, the electrons in the capacitance band are excited and migrate to the conduction band within a few femtoseconds. The electron void in the valence band is itself an electrical conductor, so this process leads to electron charge carriers and holes. If these electrons and holes are trapped

on the surface of the semiconductor and the recombination of the electron/hole pair is prevented, the following set of reactions will occur:

1- Photon excitation	$TiO_2 + hv \rightarrow e^- + h^+$
2- Trapping of free electrons	$e^-_{CB} \rightarrow e^-_{TR}$
3- Stuck holes	$h^+_{VB} \rightarrow h^+_{TR}$
4- Reassembly of charge carriers	$e^-_{TR} + h^+_{VB} \rightarrow e^-_{CB} + heat$
5- Sweeping the excited electrons	$(O_2)_{ads} + e^- \rightarrow O^-_2$
6- Hydroxyl oxidation	$OH^- + h^+ \rightarrow OH\cdot$
7- Photocatalytic degradation with hydroxyl radical	$R\text{-}H + OH\cdot \rightarrow R' + H_2O$

The hydroxyl radicals produced in step 6 convert organic impurities into intermediates, which are often converted to water and carbon dioxide as a by-product by the same reaction or reactions [45].

Biancullo *et al.* (2019) investigated the effect of a heterogeneous TiO_2 photocatalyst for the treatment of effluent from a secondary treatment system with azithromycin (AZT), trimethoprim (TMP), ofloxacin (OFL), and sulfamethoxazole (SMX). In this study, various operational parameters such as irradiation conditions, amount of catalyst, and use of methanol as a carrier solvent and radical scavenger were studied. The most efficient conditions for municipal wastewater treatment (four light emitting diodes (LEDs) symmetrically distributed and a catalyst concentration of 1 $g.L^{-1}$) were used to remove antibiotics in real conditions. The results showed that one hour of photocatalytic treatment was sufficient to reduce antibiotics to less than the allowable level [47].

Elsewhere, Ayekeo *et al.* (2019) studied the combined effect of coagulation-flocculation processes and heterogeneous photocatalytic activity to improve the removal of humic substances in water treatment from a river in Africa. In this study, heterogeneous photocatalytic activity was performed with the help of TiO_2-P25 suspended catalyst and TiO_2-P25/-SiC support material. Coagulation-flocculation and the heterogeneous photocatalytic method were used separately and together to evaluate the best removal process for organic compounds. The initial concentration of dissolved carbon (DOC) in the river water was about 20 $mg.L^{-1}$. To remove the compounds, the coagulation-flocculation process was first optimized. Optimization of the coagulation-flocculation process was achieved at $pH = 5$ with a dose of 110 $mg.L^{-1}$ of coagulant, which resulted in the removal of 70% of the humic substances. Coupling of the coagulation process and 220 minutes of photocatalytic irradiation resulted in the removal of an additional 80% of the humic substances which had remained after coagulation-flocculation. Therefore, with this combined process of coagulation-flocculation and heterogeneous photocatalytic activity, approximately 90% of the humic substances were removed [48].

1.4 APPLICATIONS OF PHOTOCATALYTIC PROCESSES

1.4.1 Water splitting

The global thirst for energy is one of the problems facing current and future generations. Among the various energy substitution strategies for fossil fuels, hydrogen is one of the main candidates; but the main problem is the lack of access to hydrogen gas in nature. Therefore, technology is needed to decompose and/or extract hydrogen from various materials which contain it, in a safe and clean manner. To this end, solar energy can be used to produce environmentally friendly hydrogen through water splitting. To be more specific, photocatalytic or photoelectrochemical water splitting techniques can be used to produce hydrogen using solar energy [49, 50].

For instance, Shi *et al.* (2019) investigated the photocatalytic effect of $Co_3(PO_4)_2$/g-C_3N_4 for hydrogen production by direct deposition of water under the effect of electrostatic colonic interaction. The presence of $Co_3(PO_4)_2$ plates increased the light absorption range of the unconventional $Co_3(PO_4)_2$/g-C_3N_4 heterostructure, and increased the contact surface which led to enhanced interfacial charge transfer between g-C_3N_4 and $Co_3(PO_4)_2$ nanoplates. The optimal heterostructure showed a maximum production rate of 375.6 and 177.4 $\mu mol.g^{-1}.h^{-1}$ for O_2 and H_2, respectively. In addition, the composite has high stability and high recyclability, which helps with the potential application of this structure for sustainable energy production [51].

1.4.2 Solar energy

The sun, as a natural nuclear reactor, releases small packets of energy, that is photons. These particles contain an enormous amount of energy that is sufficient for a large part of the earth's energy needs. Photocatalytic materials are used in various forms to absorb photon energy and generate electricity in solar cells. Many types of solar cells, such as organic, photoelectrochemical, color-sensitive, and hybrid cells, have been developed to use solar energy.

1.4.3 Reduction of carbon dioxide

It is no secret that burning fossil fuels leads to the production of CO_2, which is a greenhouse gas that slows down the escape of heat from the atmosphere into space and warms the earth. Many efforts are underway to reduce the amount of carbon dioxide in the atmosphere, including the absorption, storage and use of carbon dioxide. The conversion of CO_2 into value-added chemicals is one of the most attractive ways to reduce carbon dioxide in nature. However, the main problem with carbon dioxide conversion is its very stable structure and the high energy of the C = O bond (805 $KJ.mol^{-1}$ bond enthalpy). The use of photocatalysts to solve this problem has attracted the attention of many researchers [52]. The process mainly consists of three stages: light absorption, separation and transfer of charge carriers, and reduction reactions [53].

Wang *et al.* (2020) produced $FeCoS_2$-CoS_2 bilayer nanotubes to reduce carbon dioxide using the photocatalytic method under visible light. In the production strategy, two cation exchange steps connected two metal sulfides to a

two-shell cylindrical heterostructure, with each shell being in the form of a two-dimensional nanoplate. By using the $FeCoS_2$-CoS_2 hybrid structure, the energy required to excite the charge carriers was reduced, facilitating their separation. In addition, this composite structure increased the active photocatalytic sites to reduce carbon dioxide and increase the light absorption efficiency. As a result, this double-walled nanotube showed high activity and stability [54].

1.4.4 Water and wastewater treatment

Various types of pollutants have contaminated water resources in recent decades. Emerging organic pollutants and resistant organic and inorganic compounds are among the pollutants that conventional water and wastewater treatment processes have a hard time removing with suitable efficiency [55]. New, and sometimes costly methods, are being explored to remove these pollutants, highlighting the need for economical and effective solutions. Thus far, the application of photocatalytic methods to remove pigments, phenols, nitrogen compounds, sulfur compounds, pharmaceutical compounds, pesticides and many other compounds has been investigated [56].

1.4.4.1 Dyes

In various dyeing processes, between 1% and 20% of the total production dye is lost and enters the environment as an effluent [57, 58]. Due to the nature of dyes, conventional biological treatment methods are not very effective [59]. Under anaerobic conditions, dyes are readily converted to amino aromatic compounds [60]. The method of adsorption and coagulation will also lead to the formation of secondary pollutants. However, methods based on photocatalytic processes have shown promising results for rapid and non-selective oxidation of organic dyes [61].

Kansal *et al.* (2009) investigated the degradation of reactive black 5 (RB5) and reactive orange 4 (RO4) dyes using a heterogeneous photocatalytic process. In this study, the photocatalytic activity of various semiconductors such as TiO_2 and ZnO was investigated. The experiments were performed by changing the pH range (3–11), the amount of catalyst (0.25–1.5 $g.L^{-1}$), and the initial dye concentration. The performance of the ZnO/UV photocatalytic system was better compared to the TiO_2/UV system. Complete decolorization of RB5 with ZnO occurred after 7 min, while only 75% decomposition occurred with TiO_2 after 7 min. For RO4 at the same duration, 92% and 62% decolorization were reported, respectively [62].

1.4.4.2 Phenols

Removal of phenolic contaminants by conventional methods such as adsorption with the help of activated carbon, membrane filtration, ion exchange, and so on. leads to the production of a condensed wastewater stream during the treatment process, and as a result, secondary treatment steps will be required [63]. These additional steps incur additional costs and environmental hazards. In recent years, the process of photocatalytic oxidation to remove these pollutants has yielded promising results [64].

For example, the photocatalytic degradation of resorcinol in a ZnO batch reactor has been investigated under visible light [65]. In this study, the effect of pH on COD reduction was shown to be significant, with neutral or alkaline pH proving more suitable. Mediators of the photocatalytic reaction were identified by Fourier transform infrared spectroscopy (FTIR) and gas chromatography coupled to mass spectrometry (GC/MS), as 1,2,4-trihydroxy-benzene and 1,2,3-trihydroxy-benzene. The final results showed complete removal of resorcinol (with an initial concentration of 100 ppm) and its mineralization on the surface of the ZnO photocatalyst by sunlight [65].

Elsewhere Lam *et al.* (2013) investigated the effect of TiO_2 and ZnO suspensions to evaluate the decomposition of phenol (ReOH) with an initial concentration of 10 $mg.L^{-1}$. The results showed that under optimal conditions, the removal efficiency of the contaminant by ZnO nanoparticles was better than by TiO_2. In the mechanism of degradation of ReOH phenol by TiO_2, the participation of hydroxyl radicals and positive cavities as oxidizing species were reported, while degradation in the presence of ZnO mainly occurred due to hydroxyl radicals [66].

In another study, TiO_2/g-C_3N_4 (TCN) thin-film electrodes were used by Wei *et al.* (2017) to investigate the combined effects of electrocatalysis and photocatalysis on the oxidation of phenolic contaminants with an initial concentration of 5 $mg.L^{-1}$. The study showed that phenol was completely oxidized in the presence of TCN with 1.5 V bias for 1.5 h under simulated sunlight [67].

1.4.4.3 Nitrogen-containing compounds

Nitrogenous compounds can cause environmental problems due to their high stability and solubility in water, as well as the fact that they are nutrients which can cause eutrophication.

Wang *et al.* (2010) investigated a photocatalytic treatment method for the treatment of nitrobenzene in industrial wastewater. In this study, a new photocatalyst consisting of a layer of phosphotogenic acid ($H_3PW_{12}O_{40}$) coated on a titanium dioxide (TiO_2) substrate was used. The results showed that the reaction time, the amount of catalyst, and the concentration of nitrobenzene were the main parameters determining the degradation of the pollutant. The maximum degradation of nitrobenzene with an initial concentration of 40 $mg.L^{-1}$ in water was about 94.1% [68].

Elsewhere, Luo *et al.* (2015) synthesized and investigated the photocatalytic effect of La/Fe/TiO_2 on wastewater treatment containing ammonia nitrogen. In this study, La/Fe/TiO_2 catalyst was first synthesized using the sol-gel method. The produced composite had better chemical and physical properties in photocatalytic activity than pure TiO_2. Strong visible light response, higher contact surface, and more regular shape in morphology are some of the enhanced properties of this photocatalyst. The results of optical decomposition of ammonia nitrogen show that La/Fe/TiO_2 has higher catalytic activity for the degradation of ammonia nitrogen compared to pure TiO_2 and TiO_2 doped with a single metal. Ultimately, less than 70% of the ammonia nitrogen with an initial concentration of 100 $mg.L^{-1}$ could be removed using the developed catalyst [69].

1.4.4.4 Sulfur-containing compounds

Sulfur compounds are toxic, corrosive and odorous, which can lead to environmental hazards. In various industries, including the oil and petrochemical industries, wastewater streams containing sulfur compounds are obtained from the desulfurization process. The presence of sulfide in wastewater reduces water-soluble oxygen and consequently endangers the life of living organisms in water [70]. Also, refineries need large amounts of hydrogen to refine sulfur-rich crude oils. To solve both problems, photocatalytic methods with high oxidation potential (+2.8 V) have been proposed to mineralize organic pollutants [71].

For example, Bharatvaj *et al.* (2018) doped Cerium (Ce^{3+}) onto titanium dioxide powder with the sol-gel method in order to reduce the TiO_2 band gap from about 3.2 to 2.7 eV (visible light region). The photocatalytic activity of this compound was evaluated by treating sulfidic wastewater [72].

1.4.4.5 Pharmaceutical compounds

Drug compounds are commonly found in municipal wastewater in concentrations from nanograms to micrograms per liter [73]. Although drugs are resistant to treatment, their low levels in municipal water and wastewater will not pose an operational problem for wastewater treatment plants. However, pharmaceutical wastewater is a distinct case that contains high levels of TOC. Photocatalytic methods are among the methods that are usually recommended for the treatment of these pollutants [74].

Deng *et al.* (2018) investigated the deposition of silver nanoparticles on semiconductors to improve the separation of electron-pores produced by light due to plasma resonance. The performance efficiencies of existing Ag-based photocatalysts are still low and practical applications are yet to materialize. In this study, silver nanoparticles were coated on $AgIn_5S_8$, using a solvothermal method and photon reduction, to improve the separation of carriers and the catalytic activity in the visible light. The 2.5% $Ag/AgIn_5S_8$ nanocomposite showed the highest photocatalytic degradation efficiency with 95.3% degradation efficiency for tetracycline hydrochloride with an initial concentration of 10 $mg.L^{-1}$. The catalyst was also used for real wastewater treatment in the pharmaceutical industry and showed an acceptable rate of mineralization and COD removal [75].

Degradation of carbamazepine (CBZ) and ibuprofen (IBP) in an aqueous environment with ZnO and TiO_2 photocatalysts under ultraviolet and visible light irradiation have also been investigated [38]. The effect of different parameters on degradation efficiency such as catalyst type and loading rate (50–500 $mg.L^{-1}$), initial drug concentration (10, 40, 80 $mg.L^{-1}$), and radiation wavelength (200–600 nm) were investigated. The results showed that exposure to visible light ($\lambda_{exc} > 390$ nm) caused a complete photocatalytic degradation reaction of both compounds. Regardless of other parameters such as the type of photocatalyst, the initial drug concentration, and the wavelength of the visible light emitted, the IBP conversion reaction rate is higher than that of CBZ. The presence of isopropanol also showed a significant inhibitory effect on CBZ degradation, which is considered as evidence of the effect of the solution phase composition [76].

1.4.4.6 Pesticides

Pesticides and toxicants are major pollutants in the agro-chemical industry. In one study by Alalam *et al.* (2015), the removal of pesticides from industrial wastewater was targeted. For this, nano TiO_2 was employed, and the monitored pollutants in the samples were chlorpyrifos, lambda-cyhalothrin, and diazinon. COD was also measured as a parameter regarding the level of pollution in the wastewater. The independent variables of initial pH, irradiation time, and chemical dose were altered to observe their effects on the dependent variable. The maximum removal of COD with the photo-Fenton process was 90.7%, while with photocatalytic treatment it was 79.6% [77].

Elsewhere, Kushniarou *et al.* (2019) conducted a study to photocatalytically degrade 12 conventional pesticides for vegetables, grapes, citrus fruits, and fruit crops in an aqueous suspension of TiO_2 and $Na_2S_2O_8$ in a semi-industrial unit under natural sunlight in Murcia, Spain. The optical decomposition of all pesticides can be modeled by assuming quasi-first-order kinetics. The time required to remove 90% of the contaminants in the summer was reported to be less than 4 hours, except for cyproconazole which was reported to be 4.9 hours [78].

1.5 PHOTOCATALYTIC MATERIALS

1.5.1 Semiconductors

Semiconductors are materials of choice for photocatalysts, particularly metal oxides and metal sulfides. As stated earlier, the performances of photocatalysts are directly related to their electronic band structures. To be efficient in the visible fraction of the solar spectrum, a photocatalyst must have a band gap between 3 and 1.5 eV. Photocatalysts having band gaps between 3 and 4 eV are active in the UV range. The energy level of the conduction and valence bands also plays a crucial role. In order to generate OH· radicals the valence band should have an oxidation potential above 2.31 V/ENH (potential of the couple $OH\cdot/H^+$, H_2O), and/or the conduction band below 0.92 V/ENH (potential of the oxygen reduction in $O_2^{\cdot-}$) [6]. As presented in Figure 1.6, many semiconductors have the required properties, like ZnO [79], WO_3 [80], Fe_2O_3 [81], TiO_2 [82], SnO_2 [83], CdS [84] and CdSe [85]. With a band gap of 3.8 eV, SnO_2 is active too far in the UV range, below 325 nm. WO_3, α-Fe_2O_3, CdS and CdSe are materials active in the visible range, with band gaps between 1.7 and 2.7 eV. However, the valence band energy of CdS and CdSe does not allow the oxidation of water into OH·. Concerning α-Fe_2O_3, its small band gap and the favorable edge position of its electronic bands make it a promising material for photocatalytic degradations. However, the photocatalytic performances of a-Fe_2O_3 are limited due to the quick recombination rate of e^-/h^+ carriers and the low diffusion length of h^+ (2–4 nm) [86]. The same limitations are observed for WO_3 [87].

ZnO and TiO_2 have an identical band gap around 3.3 eV. They are the two most used and studied oxides in the literature concerning the photocatalytic degradation of pollutants in water. Indeed, they are the two most performing and reliable materials in photocatalytic water treatment. They are chemically and thermally stable, not expensive and can be synthesized easily under different forms such as nanoparticles, nanowires, thin films and so on. The position of

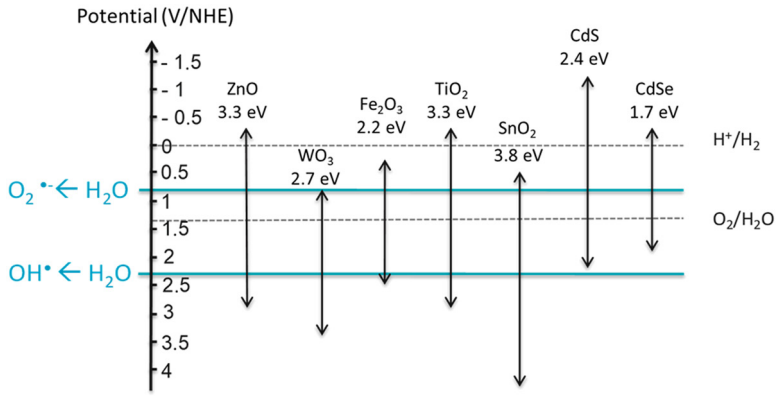

Figure 1.6 Band gaps and band positions of different semiconductors. Reprinted with permission from [4].

their bands as well as their long carrier lifetime and diffusion lengths allow them to efficiently oxidize water into OH·. Yet, these materials show photocatalytic activity in the UV range only, below 375 nm. Therefore, much effort has been made in preparing visible light active photocatalysts, by tuning ZnO and TiO_2 band structures. Reported strategies include doping with metallic (like Fe^{2+}, Co^{2+}, Ag^{+}, Cu^{2+}, and Mn^{2+}) [88] or nonmetallic elements (like N, C, S or P) [89], surface plasmon resonance [90], sensitization with dyes or association with other semiconductors like heterostructures or Z-schemes [91, 92].

1.5.2 Heterostructures

Heterostructures or heterojunctions created between different semiconductors have been studied for their ability to enhance light absorption in the visible range. Additionally, heterostructures have increased charge carrier lifetime and mobility with respect to the original semiconductors constituting the heterostructure [93]. A heterostructure is an interfacial association of two or more components. Depending on the band alignment of the semiconductors, three types of heterostructures can be created, as presented in Figure 1.7: type I (symmetric), type II (staggered) and type III (broken). Type I heterostructures promote the recombination of photogenerated electrons/holes. Consequently, they are often found in LED systems, where the radiative recombination of charge carriers must be maximized [94]. In the photocatalytic processes, type II heterostructures are particularly attractive, since they promote the separation and delocalization of photogenerated charge carriers. Thanks to a built-in electric potential created at the interface of the two semiconductors, holes are driven in the valence band (VB) of one semiconductor, while electrons are driven in the conduction band (CB) of the second one [95]. Subsequently, photogenerated charge carrier lifetimes are increased. Type III or broken heterostructures find applications in tunneling field effect transistors [96].

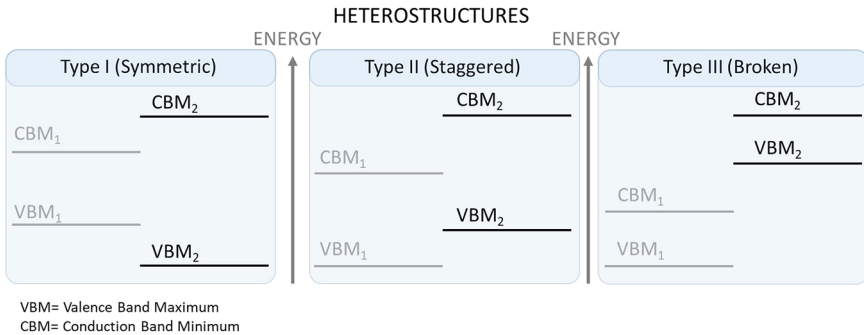

Figure 1.7 Schematic representation of the three possible types of heterostructures. Reproduced from [97].

In water treatment or hydrogen production applications, type II heterostructures between two semiconductors have been particularly investigated in the literature. This kind of junction can be created between different metal oxides, metal sulfides or carbon-based structures such as, for example, ZnO [98], TiO_2 [99], SnO_2 [100], CdS [101], WO_3 [102], and g-C_3N_4 [103]. In the case of a heterostructure like ZnO/SnO_2 (Figure 1.8), the improvement of photocatalytic properties is due to longer lifetime of charge carriers, induced by the electron/hole separation towards the opposite sides of the junction [100]: electrons are driven from the valence band of ZnO to the valence band of SnO_2, and the holes are driven from the conduction band of SnO_2 to the conduction band of ZnO. Thus, the photocatalytic degradation kinetic of methylene blue is quicker in the presence of the heterostructure. In

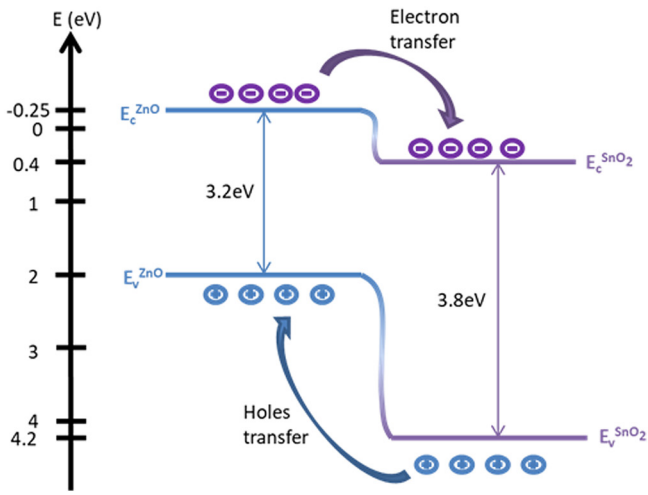

Figure 1.8 Schematic representation of charge carrier behavior in type II heterostructure ZnO/SnO_2. Reproduced from [20].

addition, thanks to its high chemical and thermal stability, SnO_2 acts also as a protective material against the degradation/dissolution of ZnO in water [97].

Other kinds of heterostructures attempt to use visible light sensitive semiconductors in order to shift the absorbance and the photocatalytic activity of the structure toward the visible range. Such heterostructures still provide efficient separation of charge carriers. Good examples of these are ZnO/CuS [104] or TiO_2/CdS [105] heterostructures. Basu *et al.* [104] demonstrated that ZnO nanotubes decorated with a CuS shell were 2.5 times more efficient for the visible light (>400 nm) photocatalytic degradation of methylene blue than CuS only. In the visible range, ZnO alone showed no activity at all. Here, the double effect of the heterostructure is highlighted: photocatalysis efficiency improvement and visible light activity.

1.5.3 Z-Scheme heterostructures

A fourth type of heterostructure, possessing similar band alignments to the type II heterostructure, is the Z-scheme heterostructure. In the case of a Z-scheme junction, the charge carriers' migration mechanism is different from that of the type II heterostructure. Holes generated in the valence band of semiconductor 'A' recombine with electrons generated in the conduction band of semiconductor 'B' as shown in Figure 1.9. Consequently, holes with the highest oxidative potential (lowest valence band) and electrons with the highest reductive potential (highest conduction band) remain available for the photocatalytic action, unlike in the type II heterostructure, where electrons and holes are driven to lower energy states.

Three different kinds of Z-schemes can be developed: the liquid phase Z-scheme, the all-solid-state Z-scheme and the direct Z-scheme (Figure 1.10). The liquid phase Z-scheme was first discovered in 1979 [107]. It is prepared by associating two different semiconductors with a shuttle redox mediator, via an electron acceptor/donor (A/D) pair like Fe^{2+}/Fe^{3+} or I^-/IO^{3-} [108]. The all-solid-state Z-scheme, the second technology developed, relies on the use of a solid electron mediator between the two semiconductors. The electron

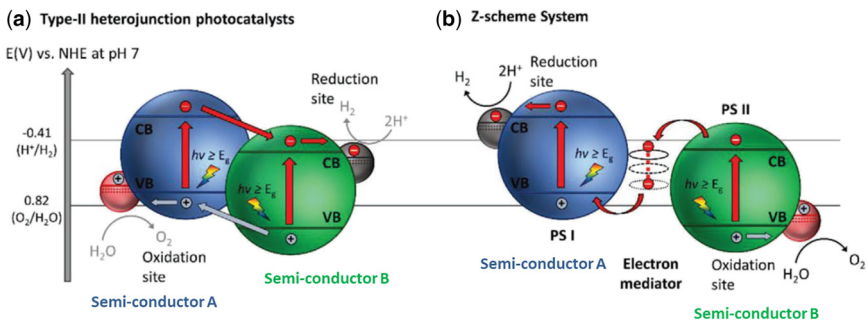

Figure 1.9 Schematic representation of carrier recombination in (a) type II heterojunction, (b) Z-scheme heterojunction. Reproduced from [106].

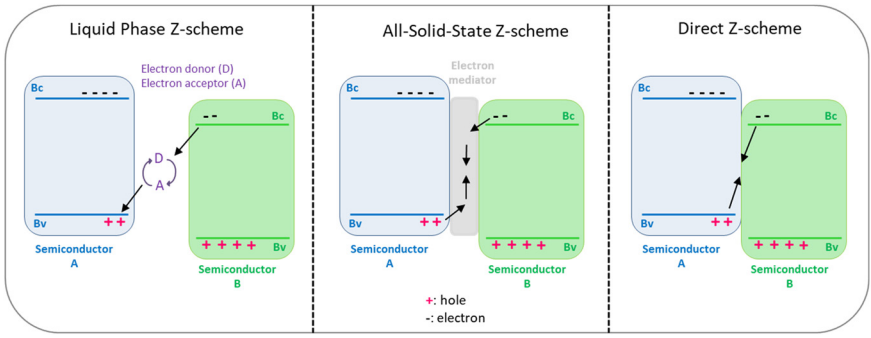

Figure 1.10 Schematic representation of the three different types of Z-scheme: the liquid phase Z-scheme, the all-solid-state Z-scheme and the direct Z-scheme.

mediator is typically a noble metal (Au, Pt, Ag) in the form of nanoparticles or a thin film, or a conductive carbon structure like graphene sheets, nanotubes or quantum dots [109–111]. More recently, the third generation of Z-scheme, the direct Z-scheme, consists of semiconductors that are both directly in contact, like in the type II heterostructure.

The difference between a type II heterostructure and a direct Z-scheme results from the electronic configuration determined by the Fermi level of the two semiconductors to couple (Figure 1.11). Graphitic carbon nitride g-C_3N_4 has a higher Fermi level than ZnO [108]. Thus, when the two materials contact, electrons from the g-C_3N_4 migrate toward the ZnO during the Fermi level alignment at the interface. The local electron depletion induces an upward band bending in the g-C_3N_4 and a downward band bending in the ZnO. As the conduction band minimum and valence band maximum of g-C_3N_4 are higher than those of ZnO, it results in the formation of a direct Z-scheme between g-C_3N_4 and ZnO. In the case of a heterojunction based on ZnO and SnO_2, the Fermi level of SnO_2 being higher than that of ZnO [112] leads to an upward band bending in the SnO_2 and a downward band bending in the ZnO. As the conduction band minimum and valence band maximum of ZnO are higher than those of SnO_2, the band bending leads to the formation of a type II heterostructure.

Huang *et al.* [113] showed that between the two semiconductors g-C_3N_4 and $W_{18}O_{49}$, a type II heterostructure or a direct Z-scheme could be obtained depending on their band bending at the interface. When the two bare materials form a junction, the Fermi level of $W_{18}O_{49}$ is higher than that of g-C_3N_4 leading to a type II heterostructure. However, if triethanolamine is adsorbed at the surface of those two materials, the Fermi level of g-C_3N_4 is upshifted above the Fermi level of $W_{18}O_{49}$, forming a direct Z-scheme junction.

Z-scheme photocatalysts are considered as a promising technological solution for visible light driven treatment of water. Indeed, just like for type II heterostructures, the association of a visible light sensitive semiconductor with an efficient photocatalyst like ZnO or TiO_2 provides photocatalysts

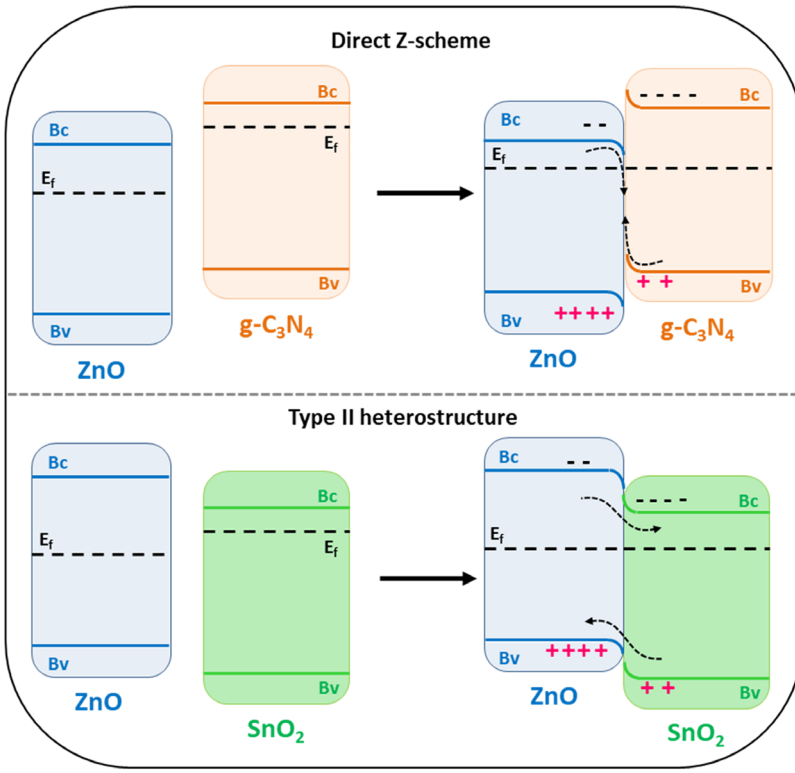

Figure 1.11 Schematic representation of the formation of type II heterostructure and direct Z-scheme between ZnO/SnO_2 and ZnO/g-C_3N_4 depending on their Fermi level energy difference.

with the possibility of working under solar light. On top of that, Z-scheme photocatalysts have an advantage over type II heterostructures, as they promote the preservation of high energy carriers in the lowest valence band and the highest conduction band. Therefore, Z-scheme photocatalysts like TiO_2/g-C_3N_4 [114], ZnO/g-C_3N_4 [115], $ZnIn_2S_4$/Bi_2WO_6 [116] or ZnO/CdS [117] have been thoroughly studied in order to prove their efficiency for photocatalytic water purification as well as for hydrogen production by water splitting.

1.6 OPERATIONAL PARAMETERS AFFECTING THE PHOTOCATALYTIC PROCESS

There are various parameters that can change the oxidation reaction rate and the efficiency of photocatalytic processes. In the following, the effect of several operating parameters are reviewed.

1.6.1 Effect of pH

One of the important parameters affecting photocatalytic processes is the effect of pH. The pH of the solution affects the degree of ionization, agglomeration, oxidation potential of the photocatalytic capacity band, and the absorption of pollutants [118]. Surface charge is one of the important parameters in the photocatalytic process that is affected by pH. The pH value at which the surface charge is completely neutralized is known as the point of zero charge (PZC). In many studies, the PZC of titanium dioxide has been used to investigate the effect of pH on its photocatalytic oxidation performance. Titanium dioxide photocatalysts have shown a PZC of 4.5 to 7, depending on the type and composition. At the PZC point, due to the lack of electrostatic force, the attraction between contaminants in water and photocatalytic particles is minimal. At pH less than PZC the surface of the photocatalyst is charged with positive charges and generates electrostatic attraction for negative charges and vice versa. The following shows the reactions of titanium dioxide with respect to the PZC [119]:

$$\mathrm{pH} < \mathrm{pH_{PZC}} \quad \mathrm{TiOH} + \mathrm{H^+} \rightarrow \mathrm{TiOH_2^+} \tag{1.18}$$

$$\mathrm{pH} > \mathrm{pH_{PZC}} \quad \mathrm{TiOH} + \mathrm{OH^-} \rightarrow \mathrm{TiO^-} + \mathrm{H_2O} \tag{1.19}$$

Sun *et al.* (2019) controlled the morphology of a $BiVO_4$ catalyst by adjusting the pH of the solution to degrade phenol-containing effluent. The results showed that the photocatalytic activity of $BiVO_4$ for phenol degradation was improved by increasing the pH value. Reasons for higher photocatalytic activity include altered morphology, higher ability to absorb sunlight, smaller band gaps, and less recombination of electron pairs [120].

In another study, Guo *et al.* (2020) investigated the photocatalytic activity of $AgBr/Ag_2CO_3$ synthesized by the in situ growth method at different pHs. The results showed that the $AgBr/Ag_2CO_3$ heterostructure had a higher photocatalytic activity than pure AgBr and Ag_2CO_3. In addition, different pH conditions (between pH 7 to 10) caused changes in photocatalytic activity due to their effect on crystallization. The $AgBr/Ag_2CO_3$ photocatalyst produced at pH = 9 had the highest photocatalytic activity and the degradation rate of rhodamine B with an initial concentration of 5 $mg.L^{-1}$ in 20 minutes was 98.93% [121].

Intaphong *et al.* (2020) investigated the effect of pH on the crystal structure, morphology and photocatalytic behavior of BiOBr under visible light. The photocatalytic properties of BiOBr with different morphologies made using the hydrothermal method were investigated for optical decomposition of rhodamine B. Hierarchical micro-flowers at pH = 8 showed the best photocatalytic activity with a decolorization efficiency of nearly 98% [122].

1.6.2 Temperature

Another important parameter that has a great impact on photocatalytic activity and degradation of pollutants is temperature. Most photocatalytic reactions take place at room temperature, however, at temperatures below

0°C, the desorption rate of the final product decreases and thus increases the activation energy. Also, by increasing the reaction temperature above 80°C, the adsorption of the reactant becomes a limiting factor [123].

Ariza-Tarazona *et al.* (2020) investigated the effect of temperature and pH on the photocatalytic degradation of microplastic contaminants with the help of carbon and nitrogen-doped titanium dioxide photocatalyst. The concentration of microplastic contaminants in the experiments was 4000 $mg.L^{-1}$. Here, low temperature (0°C) increased the surface of microplastic by means fragmentation and low pH (pH = 3) caused the formation of hydroperoxide during photooxidation [124].

Neto *et al.* (2019) investigated the photocatalytic effect of Ag_2WO_4 nanorods at different temperatures (10, 30, 50, 70, and 90°C) on the degradation of methylene blue (MB) and methyl orange (MO). The increase in temperature lengthened and reduced the thickness of the nanorods, thereby increasing their surface area, and their rate of absorption. Each photocatalyst was used in four photocatalytic cycles to accurately evaluate performance and stability [125].

1.6.3 Presence of oxidants

Oxidants (e.g. H_2O_2, $KBrO_3$, and HNO_3) are external agents that are added to the reaction as irreversible electron acceptors to help produce intermediate radicals to remove contaminants. Therefore, oxidants are electron scavengers from the valance band and increase the efficiency of the photocatalytic process by: (1) reduction of electron/hole pair recombination time, (2) increased production of OH· to destroy pollutants, and (3) production of oxidant species for increasing oxidation rates [126].

1.6.4 Pollutant concentration

Studying the relationship between pollutant concentration and the photocatalytic degradation rate is of great importance for the practical design of photocatalytic treatment units. The degradation reaction of many contaminants follows pseudo-first-order kinetics that can be corrected in the form of the Langmuir-Hinshelwood equation for solid-liquid reactions.

$$\ln\left(C_0/C\right) = k_r K t = k_1 t \tag{1.20}$$

In this equation, k_1 is the first-order reaction constant, t is the time required to reduce the concentration from the initial concentration (C_0) to the final concentration (C), K is the equilibrium constant for adsorption of the contaminant to the catalyst surface, and k_r is the reaction limiting rate [127].

In the case of color compounds, the amount of degradation may increase with increasing color concentration (because more molecules will be available for degradation), but after reaching a certain critical concentration, this amount begins to decrease. This reduction can be attributed to the reduction in the amount of ultraviolet radiation reaching the photocatalyst surface. In most studies, a concentration of pollutants in the range of 10–200 $mg.L^{-1}$ has been used, which corresponds to the amount in most real wastewater samples [128].

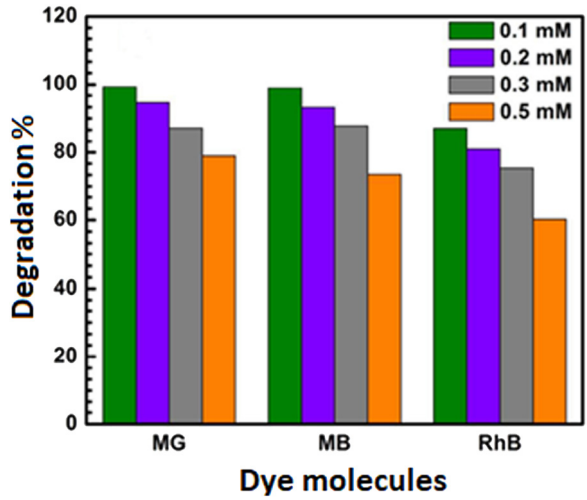

Figure 1.12 The relationship between initial pollutant concentration and photocatalytic degradation of dyes. Reprinted from [129].

Boruah *et al.* (2016) investigated the photocatalytic degradation of methyl green (MG), methyl blue (MB), and rhodamine B (RhB), and the reduction of Cr (VI) in an aqueous medium using a recyclable magnetic catalyst of Fe_3O_4/reduced-graphene-oxide (rGO) under visible light. The effect of initial pigment concentration on the rate of photocatalytic degradation was one of the important parameters investigated in this study. At a constant concentration of 0.5 $g.L^{-1}$ of photocatalyst and pH = 5, the concentration of pigment molecules was altered between 0.08 and 0.5 mM. Figure 1.12 shows that at an initial concentration of 0.1 mM, the rate of photocatalytic degradation of all three pigments is over 98%. However, the efficiency of photocatalytic degradation decreased with increasing initial photocatalyst concentration [129]. This implies that even the lowest concentration of dye might have hindered the penetration of adequate light into the solution.

Elsewhere, Chanu *et al.* (2019) investigated the effect of operating parameters on the photocatalytic degradation of methylene blue pigment by manganese doped zinc oxide (ZnO) nanoparticles. To investigate the effect of the initial concentration of the pigment, a constant concentration of catalyst (0.30 $g.L^{-1}$) and pH = 12 were used with varying pigment concentration. The graph of $\ln(C_0/C)$ versus radiation (Figure 1.13) shows the maximum amount of photocatalytic degradation at a concentration of 10 ppm. Increased degradation with increasing concentration has been attributed to increasing the probability of the dye molecules colliding with the OH· radical. Also, the reduction of the reaction rate after the optimal concentration of contaminants has been attributed to the coverage of the catalyst surface by contaminants and the reduction of the produced OH· radical [130].

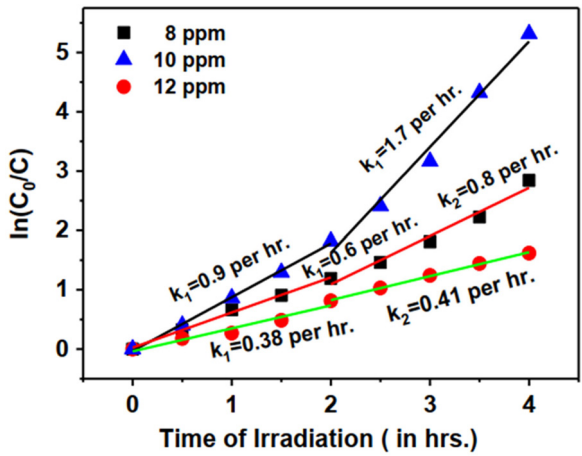

Figure 1.13 The graph of $\ln(C_0/C)$ versus time at different concentrations of dye. Reprinted from [130].

1.6.5 Catalyst loading

Increasing the amount of catalyst will logically increase active sites in the solution, resulting in more photon adsorption and greater production of OH· hydroxyl radicals and irradiated positive holes. However, an excessive increase in the amount of catalyst can reduce the amount of photocatalytic activity. One of the important reasons for this decrease in activity is the increase in solution turbidity and light scattering, which reduces the number of photons absorbed by the photocatalyst [131, 132].

Paul *et al.* (2019) investigated the effect of operational parameters on photocatalytic degradation of methylene blue (MB) by urea-based graphite nitride carbonate (g-C_3N_4). The results showed that increasing the amount of photocatalyst from 0.01 g to 0.05 g caused an increase in photocatalyst activity, which was attributed to the increase in active sites. Increasing the amount of photocatalyst beyond 0.05 g reduced the activity of the photocatalyst, and this has been attributed to the reduction of light received by the photocatalyst. Figure 1.14 shows the concentration of methylene blue relative to its initial concentration with respect to time [133].

1.6.6 Light intensity and wavelength

As stated earlier, in order for light to activate a photocatalytic substance, its energy must be at least equal to the energy of the photocatalyst band gap [132]. Creating charge carriers helps produce free radicals to destroy pollutants. Therefore, the amount of degradation is affected by the intensity of light, and the distribution of light in a photocatalytic reactor determines the efficiency of the pollutant conversion and the amount of degradation. In many studies, the amount of pollutant degradation has been shown to depend

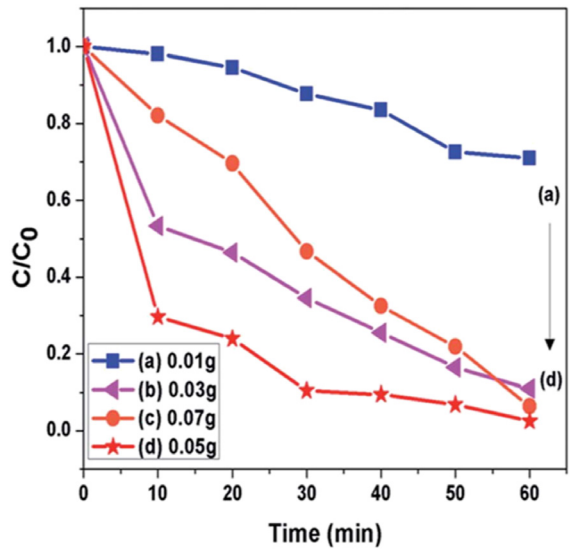

Figure 1.14 Comparison of photocatalytic activity of g-C_3N_4 with different amounts of photocatalyst loading. Initial MB concentration is 10 ppm and pH = 11. Reprinted from [133].

linearly on the intensity of the light, while in others, the relationship between the amount of degradation and the square of the light intensity is linear. It should be noted that at high intensities the reaction rate is independent of light intensity [134].

For example, in one study by Chen *et al.* (2019), carbon quantum dots were modified by $K_2Ti_6O_{13}$ nanotubes to produce a composite. It was hypothesized that this modification would help the degradation of amoxicillin under visible light. For this irradiation under wavelengths ranging from 420 to 630 nm were investigated. With increasing wavelength, the photocatalytic activity decreased due to changes in photon energy. Furthermore, the composite performed significantly more effectively compared with when $K_2Ti_6O_{13}$ was used alone[135].

Elsewhere, Rahimi Aghdam *et al.* (2018) investigated the removal of NOX by stabilized $BiFeO_3$ photocatalytic nanoparticles and the operating parameters affecting this process. In this study, $BiFeO_3$ perovskite (BFO) was synthesized by the sol-gel auto-combustion method. The gap band energy was calculated to be about 2.13 eV and the specific surface area of the prepared BFO nanostructure was 55.1 $m^2.g^{-1}$. The effect of UV radiation power from two UV lamps, 8 and 15 W, was investigated. As can be seen in Figure 1.15, the percentage of NO conversion was higher in the presence of the 15 W lamp. Logically, the higher ultraviolet light intensity can produce more electron/hole pairs, which accelerates the optical decomposition [136].

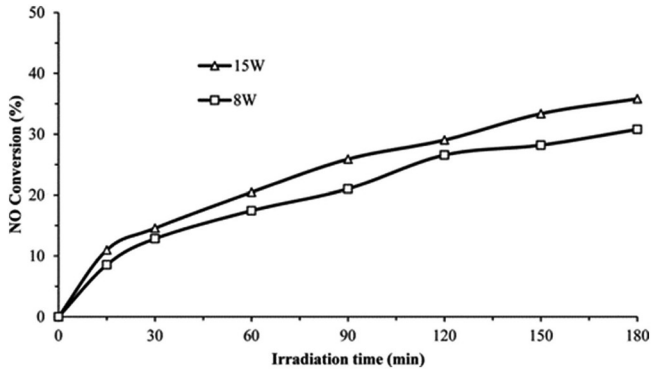

Figure 1.15 The effect of light power on photocatalytic removal performance with initial NO concentration of 5 ppm. Reprinted from [136].

1.7 CONCLUSION

This chapter has been dedicated to the introduction of photocatalytic principles and processes involved in water treatment and energy production (hydrogen/oxygen through water splitting). Mechanisms implicated in the photogeneration of charge carriers in semiconductors and charge carrier activities toward organic pollutant degradation or water splitting have been detailed. The application of photocatalytic methods to degrade multiple molecules such as dyes, phenols, nitrogen-containing molecules, pesticides and pharmaceuticals has been studied, along with characterization techniques that are able to display charge carrier lifetimes and spatial distribution in photocatalytic materials. Also, the main materials showing photocatalytic properties have been highlighted, as well as the different strategies considered to improve their photocatalytic activity. Particularly, the formation of the different heterostructures formed between semiconductors, or experimental parameters affecting the kinetic of reactions have been described.

REFERENCES

1. Ameta SC. Chapter 1 - Introduction. In: Ameta SC, Ameta R, eds. *Advanced Oxidation Processes for Waste Water Treatment*: Academic Press, Cambridge, Massachusetts, United States, 2018: 1–12.
2. Ebrahiem EE, Al-Maghrabi MN, Mobarki AR. Removal of organic pollutants from industrial wastewater by applying photo-Fenton oxidation technology. *Arabian Journal of Chemistry* 2017; **10**: S1674–S9.
3. Clarizia L, Russo D, Di Somma I, Marotta R, Andreozzi R. Homogeneous photo-Fenton processes at near neutral pH: A review. *Applied Catalysis B: Environmental* 2017; **209**: 358–71.
4. Rogé V. Etude, fabrication et caractérisation de nanostructures catalytiques de type ZnO/SnO_2 intégrées à des membranes modèles pour la dépollution de l'eau: Université de Strasbourg, 2015.
5. Rogé V, Bahlawane N, Lamblin G, *et al.* Improvement of the photocatalytic degradation property of atomic layer deposited ZnO thin films: the interplay

between film properties and functional performances. *Journal of Materials Chemistry A* 2015; **3**: 11453–61.
6. Buettner GR. The Pecking Order of Free Radicals and Antioxidants Lipid Peroxidation, α-Tocopherol, and Ascorbate. *Archives of Biochemistry and Biophysics* 1993; **300**: 535–43.
7. Maeda K. Photocatalytic water splitting using semiconductor particles: History and recent developments. *Journal of Photochemistry and Photobiology C: Photochemistry Reviews* 2011; **12**: 237–68.
8. Maeda K, Domen K. Photocatalytic Water Splitting: Recent Progress and Future Challenges. *The Journal of Physical Chemistry Letters* 2010; **1**: 2655–61.
9. Takanabe K. Photocatalytic Water Splitting: Quantitative Approaches toward Photocatalyst by Design. *ACS Catalysis* 2017; **7**: 8006–22.
10. Foglia L, Vempati S, Tanda Bonkano B, *et al.* Revealing the competing contributions of charge carriers, excitons, and defects to the non-equilibrium optical properties of ZnO. *Struct Dyn* 2019; **6**: 034501.
11. Gao Y, Nie W, Wang X, Fan F, Li C. Advanced space- and time-resolved techniques for photocatalyst studies. *Chem Commun (Camb)* 2020; **56**: 1007–21.
12. Berera R, van Grondelle R, Kennis JT. Ultrafast transient absorption spectroscopy: principles and application to photosynthetic systems. *Photosynth Res* 2009; **101**: 105–18.
13. Nakajima S, Katoh R. Time-resolved microwave conductivity study of charge carrier dynamics in commercially available TiO_2 photocatalysts. *Journal of Materials Chemistry A* 2015; **3**: 15466–72.
14. C. Colbeau-Justin MAV. Time-resolved microwave conductivity (TRMC) a useful characterization tool for charge carriers transfert in photocatalysis-a short review. *Revista Mexicana de Fisica* 2013; **59**: 191–200.
15. Tahiri Alaoui O, Herissan A, Le Quoc C, *et al.* Elaboration, charge-carrier lifetimes and activity of Pd-TiO_2 photocatalysts obtained by gamma radiolysis. *Journal of Photochemistry and Photobiology A: Chemistry* 2012; **242**: 34–43.
16. Brüninghoff R, Wenderich K, Korterik JP, Mei BT, Mul G, Huijser A. Time-Dependent Photoluminescence of Nanostructured Anatase TiO_2 and the Role of Bulk and Surface Processes. *The Journal of Physical Chemistry C* 2019; **123**: 26653–61.
17. Xing J, Chen ZP, Xiao FY, *et al.* Cu-Cu_2O-TiO_2 nanojunction systems with an unusual electron-hole transportation pathway and enhanced photocatalytic properties. *Chem Asian J* 2013; **8**: 1265–70.
18. Dillon RJ, Joo JB, Zaera F, Yin Y, Bardeen CJ. Correlating the excited state relaxation dynamics as measured by photoluminescence and transient absorption with the photocatalytic activity of Au@TiO_2 core-shell nanostructures. *Phys Chem Chem Phys* 2013; **15**: 1488–96.
19. Godin R, Wang Y, Zwijnenburg MA, Tang J, Durrant JR. Time-Resolved Spectroscopic Investigation of Charge Trapping in Carbon Nitrides Photocatalysts for Hydrogen Generation. *J Am Chem Soc* 2017; **139**: 5216–24.
20. Rogé V, Georgantzopoulou A, Mehennaoui K, *et al.* Tailoring the optical properties of ZnO nano-layers and their effect on in vitro biocompatibility. *RSC Advances* 2015; **5**: 97635–47.
21. Zhang Y, Zhang Y, Song L, *et al.* Illustration of charge transfer in graphene-coated hexagonal ZnO photocatalysts using Kelvin probe force microscopy. *RSC Advances* 2018; **8**: 885–94.
22. Zhu J, Fan F, Chen R, An H, Feng Z, Li C. Direct Imaging of Highly Anisotropic Photogenerated Charge Separations on Different Facets of a Single $BiVO_4$ Photocatalyst. *Angew Chem Int Ed Engl* 2015; **54**: 9111–4.

23. Jian A, Feng K, Jia H, Zhang Q, Sang S, Zhang X. Quantitative investigation of plasmonic hot-electron injection by KPFM. *Applied Surface Science* 2019; **492**: 644–50.
24. Marrese M, Guarino V, Ambrosio L. Atomic Force Microscopy: A Powerful Tool to Address Scaffold Design in Tissue Engineering. *J Funct Biomater* 2017; **8**(1): 7.
25. Yu W, Fu HJ, Mueller T, Brunschwig BS, Lewis NS. Atomic force microscopy: Emerging illuminated and operando techniques for solar fuel research. *J Chem Phys* 2020; **153**: 020902.
26. Eichhorn J, Kastl C, Cooper JK, *et al.* Nanoscale imaging of charge carrier transport in water splitting photoanodes. *Nat Commun* 2018; **9**: 2597.
27. Viswanathan B. Photocatalytic Degradation of Dyes: An Overview. *Current Catalysis* 2018; **7**: 99–121.
28. Rogé V, Guignard C, Lamblin G, *et al.* Photocatalytic degradation behavior of multiple xenobiotics using MOCVD synthesized ZnO nanowires. *Catalysis Today* 2018; **306**: 215–22.
29. Dashairya L, Mehta A, Saha P, Basu S. Visible-light-induced enhanced photocatalytic degradation of Rhodamine-B dye using BixSb2-xS3 solid-solution photocatalysts. *J Colloid Interface Sci* 2020; **561**: 71–82.
30. Lee SY, Kang D, Jeong S, Do HT, Kim JH. Photocatalytic Degradation of Rhodamine B Dye by TiO_2 and Gold Nanoparticles Supported on a Floating Porous Polydimethylsiloxane Sponge under Ultraviolet and Visible Light Irradiation. *ACS Omega* 2020; **5**: 4233–41.
31. Bayomie OS, Kandeel H, Shoeib T, Yang H, Youssef N, El-Sayed MMH. Novel approach for effective removal of methylene blue dye from water using fava bean peel waste. *Sci Rep* 2020; **10**: 7824.
32. Li M, Guan R, Li J, *et al.* Photocatalytic Performance and Mechanism Research of Ag/HSTiO2 on Degradation of Methyl Orange. *ACS Omega* 2020; **5**: 21451–7.
33. Bahrudin NN, Nawi MA, Nawawi WI. Enhanced photocatalytic decolorization of methyl orange dye and its mineralization pathway by immobilized TiO2/polyaniline. *Research on Chemical Intermediates* 2019; **45**: 2771–95.
34. Pino E, Calderon C, Herrera F, Cifuentes G, Arteaga G. Photocatalytic Degradation of Aqueous Rhodamine 6G Using Supported TiO_2 Catalysts. A Model for the Removal of Organic Contaminants From Aqueous Samples. *Front Chem* 2020; **8**: 365.
35. Hu C, Yu JC, Hao Z, Wong PK. Photocatalytic degradation of triazine-containing azo dyes in aqueous TiO_2 suspensions. *Applied Catalysis B: Environmental* 2003; **42**: 47–55.
36. Konstantinou IK, Albanis TA. TiO_2-assisted photocatalytic degradation of azo dyes in aqueous solution: kinetic and mechanistic investigations. *Applied Catalysis B: Environmental* 2004; **49**: 1–14.
37. Divya N, Bansal A, Jana AK. Photocatalytic degradation of azo dye Orange II in aqueous solutions using copper-impregnated titania. *International Journal of Environmental Science and Technology* 2013; **10**: 1265–74.
38. Islam MR, Islam JB, Furukawa M, Tateishi I, Katsumata H, Kaneco S. Photocatalytic Degradation of a Systemic Herbicide: Picloram from Aqueous Solution Using Titanium Oxide (TiO_2) under Sunlight. *ChemEngineering* 2020; **4**(4): 58.
39. Nguyen TT, Nam SN, Kim J, Oh J. Photocatalytic degradation of dissolved organic matter under ZnO-catalyzed artificial sunlight irradiation system. *Sci Rep* 2020; **10**: 13090.
40. Balcioglu IA, Arslan I, Sacan MT. Homogenous and Heterogenous Advanced Oxidation of Two Commercial Reactive Dyes. *Environmental Technology* 2001; **22**: 813–22.

41. Fenton HJH. LXXIII.—Oxidation of tartaric acid in presence of iron. *Journal of the Chemical Society, Transactions* 1894; **65**: 899–910.
42. Barbot E, Vidic NS, Gregory KB, Vidic RD. Spatial and Temporal Correlation of Water Quality Parameters of Produced Waters from Devonian-Age Shale following Hydraulic Fracturing. *Environmental Science & Technology* 2013; **47**: 2562–9.
43. Walling C, Goosen A. Mechanism of the ferric ion catalyzed decomposition of hydrogen peroxide. Effect of organic substrates. *Journal of the American Chemical Society* 1973; **95**: 2987–91.
44. Ahile UJ, Wuana RA, Itodo AU, Sha'Ato R, Malvestiti JA, Dantas RF. Are iron chelates suitable to perform photo-Fenton at neutral pH for secondary effluent treatment? *Journal of Environmental Management* 2021; **278**: 111566.
45. Ahmed SN, Haider W. Heterogeneous photocatalysis and its potential applications in water and wastewater treatment: a review. *Nanotechnology* 2018; **29**: 342001.
46. Malato S, Fernández-Ibáñez P, Maldonado MI, Blanco J, Gernjak W. Decontamination and disinfection of water by solar photocatalysis: Recent overview and trends. *Catalysis Today* 2009; **147**: 1–59.
47. Biancullo F, Moreira NFF, Ribeiro AR, *et al.* Heterogeneous photocatalysis using UVA-LEDs for the removal of antibiotics and antibiotic resistant bacteria from urban wastewater treatment plant effluents. *Chemical Engineering Journal* 2019; **367**: 304–13.
48. Ayekoe CYP, Robert D, Lanciné DG. Combination of coagulation-flocculation and heterogeneous photocatalysis for improving the removal of humic substances in real treated water from Agbô River (Ivory-Coast). *Catalysis Today* 2017; **281**: 2–13.
49. Kawawaki T, Mori Y, Wakamatsu K, *et al.* Controlled colloidal metal nanoparticles and nanoclusters: recent applications as cocatalysts for improving photocatalytic water-splitting activity. *Journal of Materials Chemistry A* 2020; **8**: 16081–113.
50. Luo H, Zeng Z, Zeng G, *et al.* Recent progress on metal-organic frameworks based- and derived-photocatalysts for water splitting. *Chemical Engineering Journal* 2020; **383**: 123196.
51. Shi W, Li M, Huang X, Ren H, Yan C, Guo F. Facile synthesis of 2D/2D $Co_3(PO_4)_2$/g-C_3N_4 heterojunction for highly photocatalytic overall water splitting under visible light. *Chemical Engineering Journal* 2020; **382**: 122960.
52. Li D, Kassymova M, Cai X, Zang S-Q, Jiang H-L. Photocatalytic CO_2 reduction over metal-organic framework-based materials. *Coordination Chemistry Reviews* 2020; **412**: 213262.
53. White JL, Baruch MF, Pander JE, *et al.* Light-Driven Heterogeneous Reduction of Carbon Dioxide: Photocatalysts and Photoelectrodes. *Chemical Reviews* 2015; **115**: 12888–935.
54. Wang Y, Wang S, Zhang SL, Lou XW. Formation of Hierarchical $FeCoS_2$–CoS_2 Double-Shelled Nanotubes with Enhanced Performance for Photocatalytic Reduction of CO_2. *Angewandte Chemie International Edition* 2020; **59**: 11918–22.
55. Vasilachi IC, Asiminicesei DM, Fertu DI, Gavrilescu M. Occurrence and Fate of Emerging Pollutants in Water Environment and Options for Their Removal. *Water* 2021; **13**(2): 181.
56. Ameta R, Ameta SC. *Photocatalysis: Principles and Applications*: CRC Press LLC, Boca Raton, Florida, United States, 2019.
57. Han F, Kambala VSR, Srinivasan M, Rajarathnam D, Naidu R. Tailored titanium dioxide photocatalysts for the degradation of organic dyes in wastewater treatment: A review. *Applied Catalysis A: General* 2009; **359**: 25–40.

58. Houas A, Lachheb H, Ksibi M, Elaloui E, Guillard C, Herrmann J-M. Photocatalytic degradation pathway of methylene blue in water. *Applied Catalysis B: Environmental* 2001; **31**: 145–57.
59. Arslan I, Balcioğlu IA. Degradation of commercial reactive dyestuffs by heterogenous and homogenous advanced oxidation processes: a comparative study. *Dyes and Pigments* 1999; **43**: 95–108.
60. Weber EJ, Adams RL. Chemical- and Sediment-Mediated Reduction of the Azo Dye Disperse Blue 79. *Environmental Science & Technology* 1995; **29**: 1163–70.
61. Qi X-H, Zhuang Y-Y, Yuan Y-C, Gu W-X. Decomposition of aniline in supercritical water. *Journal of Hazardous Materials* 2002; **90**: 51–62.
62. Kansal SK, Kaur N, Singh S. Photocatalytic Degradation of Two Commercial Reactive Dyes in Aqueous Phase Using Nanophotocatalysts. *Nanoscale Research Letters* 2009; **4**: 709.
63. Eriksson E, Baun A, Mikkelsen PS, Ledin A. Risk assessment of xenobiotics in stormwater discharged to Harrestrup Å, Denmark. *Desalination* 2007; **215**: 187–97.
64. Ahmed S, Rasul MG, Martens WN, Brown R, Hashib MA. Heterogeneous photocatalytic degradation of phenols in wastewater: A review on current status and developments. *Desalination* 2010; **261**: 3–18.
65. Pardeshi SK, Patil AB. Solar photocatalytic degradation of resorcinol a model endocrine disrupter in water using zinc oxide. *Journal of Hazardous Materials* 2009; **163**: 403–9.
66. Lam S-M, Sin J-C, Abdullah AZ, Mohamed AR. Photocatalytic degradation of resorcinol, an endocrine disrupter, by TiO_2 and ZnO suspensions. *Environmental Technology* 2013; **34**: 1097–106.
67. Wei Z, Liang F, Liu Y, *et al.* Photoelectrocatalytic degradation of phenol-containing wastewater by TiO_2/g-C3N4 hybrid heterostructure thin film. *Applied Catalysis B: Environmental* 2017; **201**: 600–6.
68. Weiping W, Yongkui H, Shuijin Y. Photocatalytic degradation of nitrobenzene wastewater with $H_3PW_{12}O_{40}/TiO_2$ *2010 International Conference on Mechanic Automation and Control Engineering* 2010: 1303–5.
69. Luo X, Chen C, Yang J, *et al.* Characterization of La/Fe/TiO_2 and Its Photocatalytic Performance in Ammonia Nitrogen Wastewater. *International Journal of Environmental Research and Public Health* 2015; **12**(11): 14626–14639.
70. Poulton SW, Krom MD, Rijn JV, Raiswell R. The use of hydrous iron (III) oxides for the removal of hydrogen sulphide in aqueous systems. *Water Research* 2002; **36**: 825–34.
71. Diya'uddeen BH, Daud WMAW, Abdul Aziz AR. Treatment technologies for petroleum refinery effluents: A review. *Process Safety and Environmental Protection* 2011; **89**: 95–105.
72. Bharatvaj J, Preethi V, Kanmani S. Hydrogen production from sulphide wastewater using Ce^{3+}–TiO_2 photocatalysis. *International Journal of Hydrogen Energy* 2018; **43**: 3935–45.
73. Rizzo L, Meric S, Guida M, Kassinos D, Belgiorno V. Heterogenous photocatalytic degradation kinetics and detoxification of an urban wastewater treatment plant effluent contaminated with pharmaceuticals. *Water Research* 2009; **43**: 4070–8.
74. Iervolino G, Zammit I, Vaiano V, Rizzo L. Limitations and Prospects for Wastewater Treatment by UV and Visible-Light-Active Heterogeneous Photocatalysis: A Critical Review. *Topics in Current Chemistry* 2019; **378**: 7.
75. Deng F, Zhao L, Luo X, Luo S, Dionysiou DD. Highly efficient visible-light photocatalytic performance of Ag/AgIn5S8 for degradation of tetracycline hydrochloride and treatment of real pharmaceutical industry wastewater. *Chemical Engineering Journal* 2018; **333**: 423–33.

76. Georgaki I, Vasilaki E, Katsarakis N. A Study on the Degradation of Carbamazepine and Ibuprofen by TiO_2 & ZnO Photocatalysis upon UV/Visible-Light Irradiation. *American Journal of Analytical Chemistry* 2014; **05**: 518–34.
77. Gar Alalm M, Tawfik A, Ookawara S. Comparison of solar TiO_2 photocatalysis and solar photo-Fenton for treatment of pesticides industry wastewater: Operational conditions, kinetics, and costs. *Journal of Water Process Engineering* 2015; **8**: 55–63.
78. Kushniarou A, Garrido I, Fenoll J, *et al.* Solar photocatalytic reclamation of agro-waste water polluted with twelve pesticides for agricultural reuse. *Chemosphere* 2019; **214**: 839–45.
79. Rodrigues J, Hatami T, Rosa JM, Tambourgi EB, Mei LHI. Photocatalytic degradation using ZnO for the treatment of RB 19 and RB 21 dyes in industrial effluents and mathematical modeling of the process. *Chemical Engineering Research and Design* 2020; **153**: 294–305.
80. Liu Y, Zeng X, Easton CD, *et al.* An in situ assembled WO_3–TiO_2 vertical heterojunction for enhanced Z-scheme photocatalytic activity. *Nanoscale* 2020; **12**: 8775–84.
81. Hitam CNC, Jalil AA. A review on exploration of Fe_2O_3 photocatalyst towards degradation of dyes and organic contaminants. *Journal of Environmental Management* 2020; **258**: 110050.
82. Ishchenko OM, Lamblin G, Guillot J, *et al.* Mesoporous TiO_2 anatase films for enhanced photocatalytic activity under UV and visible light. *RSC Advances* 2020; **10**: 38233–43.
83. Ma CM, Hong GB, Lee SC. Facile Synthesis of Tin Dioxide Nanoparticles for Photocatalytic Degradation of Congo Red Dye in Aqueous Solution. *Catalysts* 2020; **10**(7): 792.
84. Nasir JA, Rehman Zu, Shah SNA, Khan A, Butler IS, Catlow CRA. Recent developments and perspectives in CdS-based photocatalysts for water splitting. *Journal of Materials Chemistry A* 2020; **8**: 20752–80.
85. Sun C, Li T, Wen W, Luo X, Zhao L. ZnSe/CdSe core–shell nanoribbon arrays for photocatalytic applications. *CrystEngComm* 2020; **22**: 895–904.
86. Mishra M, Chun D-M. α-Fe_2O_3 as a photocatalytic material: A review. *Applied Catalysis A: General* 2015; **498**: 126–41.
87. Liu M, Li H, Zeng Y. Facile Preparation of Efficient WO_3 Photocatalysts Based on Surface Modification. *Journal of Nanomaterials* 2015; **2015**: 1–7.
88. Vallejo W, Cantillo A, Díaz-Uribe C. Methylene Blue Photodegradation under Visible Irradiation on Ag-Doped ZnO Thin Films. *International Journal of Photoenergy* 2020; **2020**: 1–11.
89. Lavand AB, Malghe YS. Synthesis, characterization and visible light photocatalytic activity of carbon and iron modified ZnO. *Journal of King Saud University - Science* 2018; **30**: 65–74.
90. Yasmeen H, Zada A, Ali S, *et al.* Visible light-excited surface plasmon resonance charge transfer significantly improves the photocatalytic activities of ZnO semiconductor for pollutants degradation. *Journal of the Chinese Chemical Society* 2020; **67**: 1611–7.
91. Zhen Y, Yang C, Shen H, *et al.* Photocatalytic performance and mechanism insights of a S-scheme g-C_3N_4/Bi_2MoO_6 heterostructure in phenol degradation and hydrogen evolution reactions under visible light. *Phys Chem Chem Phys* 2020; **22**: 26278–88.
92. Reginato G, Zani L, Calamante M, Mordini A, Dessì A. Dye-Sensitized Heterogeneous Photocatalysts for Green Redox Reactions. *European Journal of Inorganic Chemistry* 2020; **2020**: 899–917.

93. Kumar SG, Devi LG. Review on modified TiO_2 photocatalysis under UV/visible light: selected results and related mechanisms on interfacial charge carrier transfer dynamics. *J Phys Chem A* 2011; **115**: 13211–41.
94. Wang S, Tian H, Ren C, Yu J, Sun M. Electronic and optical properties of heterostructures based on transition metal dichalcogenides and graphene-like zinc oxide. *Sci Rep* 2018; **8**: 12009.
95. Angel RD, Durán-Álvarez JC, Zanella R. TiO_2-Low Band Gap Semiconductor Heterostructures for Water Treatment Using Sunlight-Driven Photocatalysis. In: Dongfang Y, ed. *Titanium Dioxide - Material for a Sustainable Environment*, IntechOpen, London, UK, 2018.
96. Koswatta SO, Koester SJ, Haensch W. On the Possibility of Obtaining MOSFET-Like Performance and Sub-60-mV/dec Swing in 1-D Broken-Gap Tunnel Transistors. *IEEE Transactions on Electron Devices* 2010; **57**: 3222–30.
97. Rogé V, Didierjean J, Crêpellière J, *et al*. Tuneable Functionalization of Glass Fibre Membranes with ZnO/SnO_2 Heterostructures for Photocatalytic Water Treatment: Effect of SnO_2 Coverage Rate on the Photocatalytic Degradation of Organics. *Catalysts* 2020; **10**(7): 733.
98. Mahala C, Sharma MD, Basu M. Type-II Heterostructure of ZnO and Carbon Dots Demonstrates Enhanced Photoanodic Performance in Photoelectrochemical Water Splitting. *Inorganic Chemistry* 2020; **59**: 6988–99.
99. Enesca A, Andronic L. The Influence of Photoactive Heterostructures on the Photocatalytic Removal of Dyes and Pharmaceutical Active Compounds: A Mini-Review. *Nanomaterials* 2020; **10**(9): 1766.
100. Uddin MT, Hoque ME, Chandra Bhoumick M. Facile one-pot synthesis of heterostructure SnO_2/ZnO photocatalyst for enhanced photocatalytic degradation of organic dye. *RSC Advances* 2020; **10**: 23554–65.
101. Wang G, Geng L, Tang W, *et al*. Two dimensional CdS/ZnO type-II heterostructure used for photocatalytic water-splitting. *Nanotechnology* 2020; **31**: 485701.
102. Wang Y, Chen C, Tian W, Xu W, Li L. Designing WO_3/$CdIn_2S_4$ type-II heterojunction with both efficient light absorption and charge separation for enhanced photoelectrochemical water splitting. *Nanotechnology* 2019; **30**: 495402.
103. Chen H, Xie Y, Sun X, *et al*. Efficient charge separation based on type-II g-C_3N_4/TiO_2-B nanowire/tube heterostructure photocatalysts. *Dalton Transactions* 2015; **44**: 13030–9.
104. Basu M, Garg N, Ganguli AK. A type-II semiconductor (ZnO/CuS heterostructure) for visible light photocatalysis. *J. Mater. Chem. A* 2014; **2**: 7517–25.
105. Nyamukamba P, Moloto MJ, Mungondori H. Visible Light-Active CdS/TiO_2 Hybrid Nanoparticles Immobilized on Polyacrylonitrile Membranes for the Photodegradation of Dyes in Water. *Journal of Nanotechnology* 2019; **2019**: 1–10.
106. Ng BJ, Putri LK, Kong XY, Teh YW, Pasbakhsh P, Chai SP. Z-Scheme Photocatalytic Systems for Solar Water Splitting. *Adv Sci (Weinh)* 2020; **7**: 1903171.
107. Bard AJ. Photoelectrochemistry and heterogeneous photo-catalysis at semiconductors. *Journal of Photochemistry* 1979; **10**: 59–75.
108. Low J, Jiang C, Cheng B, Wageh S, Al-Ghamdi AA, Yu J. A Review of Direct Z-Scheme Photocatalysts. *Small Methods* 2017; **1**: 1700080.
109. Pan Z, Zhang G, Wang X. Polymeric Carbon Nitride/Reduced Graphene Oxide/Fe_2O_3: All-Solid-State Z-Scheme System for Photocatalytic Overall Water Splitting. *Angew Chem Int Ed Engl* 2019; **58**: 7102–6.
110. Osaki J, Yoda M, Takashima T, Irie H. Selective loading of platinum or silver cocatalyst onto a hydrogen-evolution photocatalyst in a silver-mediated all solid-state Z-scheme system for enhanced overall water splitting. *RSC Advances* 2019; **9**: 41913–7.

111. Ng B-J, Putri LK, Tan L-L, Pasbakhsh P, Chai S-P. All-solid-state Z-scheme photocatalyst with carbon nanotubes as an electron mediator for hydrogen evolution under simulated solar light. *Chemical Engineering Journal* 2017; **316**: 41–9.
112. Wang L, Li J, Wang Y, *et al.* Construction of 1D SnO_2-coated ZnO nanowire heterojunction for their improved n-butylamine sensing performances. *Sci Rep* 2016; **6**: 35079.
113. Huang Z-F, Song J, Wang X, *et al.* Switching charge transfer of $C_3N_4/W_{18}O_{49}$ from type-II to Z-scheme by interfacial band bending for highly efficient photocatalytic hydrogen evolution. *Nano Energy* 2017; **40**: 308–16.
114. Lin H, Zhao L. Novel g-C_3N_4/TiO_2 nanorods with enhanced photocatalytic activity for water treatment and H2 production. *Journal of Materials Science: Materials in Electronics* 2019; **30**: 18191–9.
115. Paul DR, Gautam S, Panchal P, Nehra SP, Choudhary P, Sharma A. ZnO-Modified g-C_3N_4: A Potential Photocatalyst for Environmental Application. *ACS Omega* 2020; **5**: 3828–38.
116. Jo W-K, Lee JY, Natarajan TS. Fabrication of hierarchically structured novel redox-mediator-free $ZnIn_2S_4$ marigold flower/Bi_2WO_6 flower-like direct Z-scheme nanocomposite photocatalysts with superior visible light photocatalytic efficiency. *Physical chemistry chemical physics : PCCP* 2016; **18**: 1000–16.
117. Wang S, Zhu B, Liu M, Zhang L, Yu J, Zhou M. Direct Z-scheme ZnO/CdS hierarchical photocatalyst for enhanced photocatalytic H_2-production activity. *Applied Catalysis B: Environmental* 2019; **243**: 19–26.
118. Venkatachalam N, Palanichamy M, Arabindoo B, Murugesan V. Enhanced photocatalytic degradation of 4-chlorophenol by Zr^{4+} doped nano TiO_2. *Journal of Molecular Catalysis A: Chemical* 2007; **266**: 158–65.
119. Roushenas P, Ong ZC, Ismail Z, *et al.* Operational parameters effects on photocatalytic reactors of wastewater pollutant: a review. *Desalination and Water Treatment* 2018; **120**: 109–18.
120. Sun M, Guo P, Wang M, Ren F. The effect of pH on the photocatalytic performance of $BiVO_4$ for phenol mine sewage degradation under visible light. *Optik* 2019; **179**: 672–9.
121. Guo M, Wang L, Cai Y, *et al.* Effect of pH Value on Photocatalytic Performance and Structure of AgBr/Ag_2CO_3 Heterojunctions Synthesized by an In Situ Growth Method. *Journal of Electronic Materials* 2020; **49**: 3301–8.
122. Intaphong P, Phuruangrat A, Karthik K, Dumrongrojthanath P, Thongtem T, Thongtem S. Effect of pH on Phase, Morphology and Photocatalytic Properties of BiOBr Synthesized by Hydrothermal Method. *Journal of Inorganic and Organometallic Polymers and Materials* 2020; **30**: 714–21.
123. Herrmann J-M. Fundamentals and misconceptions in photocatalysis. *Journal of Photochemistry and Photobiology A: Chemistry* 2010; **216**: 85–93.
124. Ariza-Tarazona MC, Villarreal-Chiu JF, Hernández-López JM, *et al.* Microplastic pollution reduction by a carbon and nitrogen-doped TiO_2: Effect of pH and temperature in the photocatalytic degradation process. *Journal of Hazardous Materials* 2020; **395**: 122632.
125. Andrade Neto NF, Oliveira PM, Bomio MRD, Motta FV. Effect of temperature on the morphology and optical properties of Ag_2WO_4 obtained by the co-precipitation method: Photocatalytic activity. *Ceramics International* 2019; **45**: 15205–12.
126. Wang Y, Hong C-S. Effect of hydrogen peroxide, periodate and persulfate on photocatalysis of 2-chlorobiphenyl in aqueous TiO_2 suspensions. *Water Research* 1999; **33**: 2031–6.

127. Boarini P, Carassiti V, Maldotti A, Amadelli R. Photocatalytic Oxygenation of Cyclohexane on Titanium Dioxide Suspensions: Effect of the Solvent and of Oxygen. *Langmuir* 1998; **14**: 2080–5.
128. Vinu R, Madras G. Photocatalytic Degradation of Water Pollutants Using Nano-TiO_2. In: Zang L, ed. *Energy Efficiency and Renewable Energy Through Nanotechnology. Green Energy and Technology*: Springer, London, 2011: 625–77.
129. Boruah PK, Borthakur P, Darabdhara G, *et al*. Sunlight assisted degradation of dye molecules and reduction of toxic Cr(vi) in aqueous medium using magnetically recoverable Fe_3O_4/reduced graphene oxide nanocomposite. *RSC Advances* 2016; **6**: 11049–63.
130. Anju Chanu L, Joychandra Singh W, Jugeshwar Singh K, Nomita Devi K. Effect of operational parameters on the photocatalytic degradation of Methylene blue dye solution using manganese doped ZnO nanoparticles. *Results in Physics* 2019; **12**: 1230–7.
131. Fosso-Kankeu E, Pandey S, Sinha Ray S. *Photocatalysts in Advanced Oxidation Processes for Wastewater Treatment*: Scrivener Publishing LLC, Beverly, Massachusetts, United States, 2020.
132. Sohrabnezhad S, Pourahmad A, Radaee E. Photocatalytic degradation of basic blue 9 by CoS nanoparticles supported on AlMCM-41 material as a catalyst. *J Hazard Mater* 2009; **170**: 184–90.
133. Paul DR, Sharma R, Nehra SP, Sharma A. Effect of calcination temperature, pH and catalyst loading on photodegradation efficiency of urea derived graphitic carbon nitride towards methylene blue dye solution. *RSC Advances* 2019; **9**: 15381–91.
134. Terzian R, Serpone N. Heterogeneous photocatalyzed oxidation of creosote components: mineralization of xylenols by illuminated TiO_2 in oxygenated aqueous media. *Journal of Photochemistry and Photobiology A: Chemistry* 1995; **89**: 163–75.
135. Chen Q, Chen L, Qi J, *et al*. Photocatalytic degradation of amoxicillin by carbon quantum dots modified $K_2Ti_6O_{13}$ nanotubes: Effect of light wavelength. *Chinese Chemical Letters* 2019; **30**: 1214–8.
136. Aghdam TR, Mehrizadeh H, Salari D, Tseng H-H, Niaei A, Amini A. Photocatalytic removal of NOx over immobilized $BiFeO_3$ nanoparticles and effect of operational parameters. *Korean Journal of Chemical Engineering* 2018; **35**: 994–9.